Supporting Information for

New pentlandite-like oxide semiconductors $IrIn_6XYO_8$ (*X*=Ga, In; *Y*=Ge, Sn, Ti) as potential candidates for photocatalytic water splitting under visible-light irradiation

Xiaohui Yang,[b,#] Dan Liu,[c,#] Shiyu Lu,[a] Siyu Xiang,[a] Han Zhang,[a] Qian Yang,[a] Yongjiang Di,[a] Yilong Ma,[a] Rong Wang,[a,*]

[a] School of Metallurgy and Materials Engineering, Chongqing University of Science & Technology, Chongqing 401331, People's Republic of China

[b] Chongqing Institute of Green and Intelligent Technology, Chinese Academy of Sciences, Chongqing 400714, People's Republic of China

[c] Key Laboratory of Bio-based Material Science & Technology, Northeast Forestry University, Harbin 150040, People's Republic of China

[*] Corresponding author: rongwang@cqust.edu.cn

[#] The authors contributed equally to this work.

Table of Contents

1. Phonon dispersion curves of $IrIn_6XYO_8$ (X = Ga, In; Y = Ge, Sn, Ti)

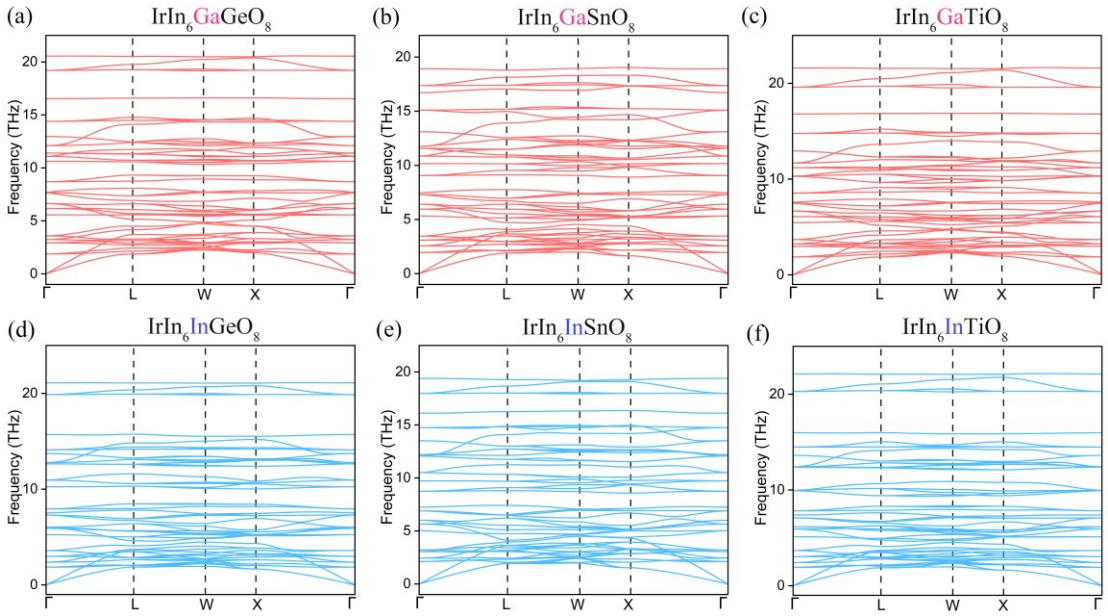

Figure S1. Calculated phonon dispersion curves of $PtIn_6GaGeO_8$ (a), $PtIn_6GaSnO_8$ (b), $PtIn_6GaTiO_8$ (c), $PtIn_6InGeO_8$ (d), $PtIn_6InSnO_8$ (e), and $PtIn_6InTiO_8$ (f).

2. Variation of energy and temperature against time for the AIMD simulation of $IrIn_6GaGeO_8$

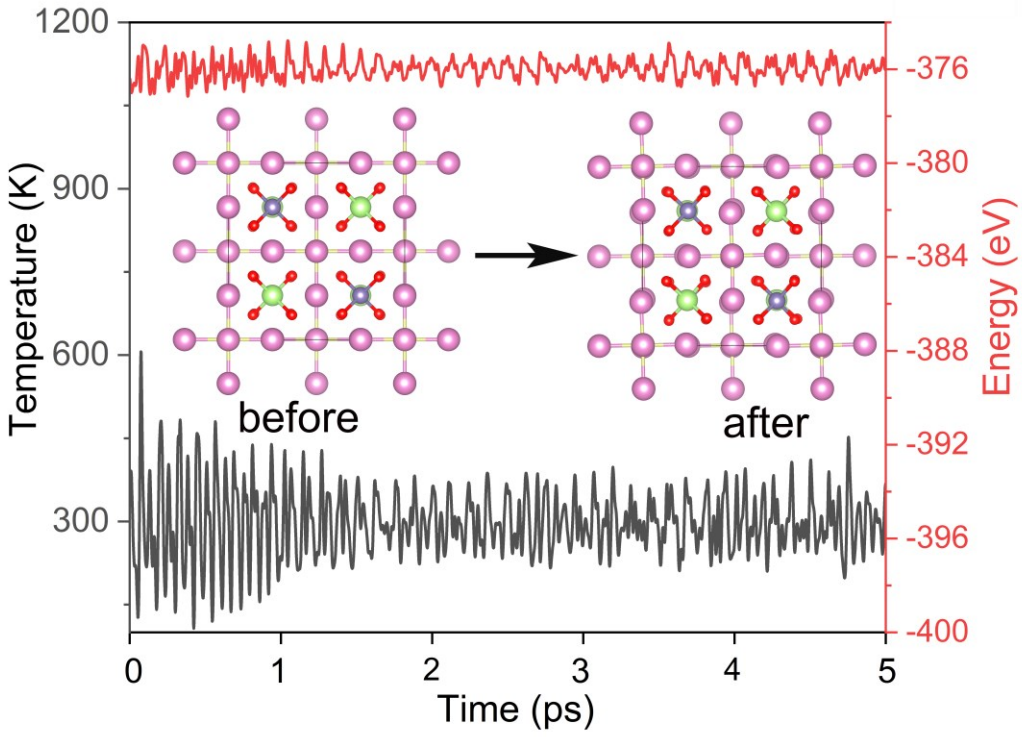

Figure S2. Fluctuations of total energy (red) and temperature T (black) during AIMD (ab initio molecular dynamics) simulations at 300 K. Insets show the crystal structures of $IrIn_6GaGeO_8$ at 0 and 5 ps of AIMD simulations. The golden, violet, pale green, gray, and red balls represent the Ir, In, Ga, Ge, and O atoms, respectively.

3. Variation of energy and temperature against time for the AIMD simulation of $IrIn_6GaSnO_8$

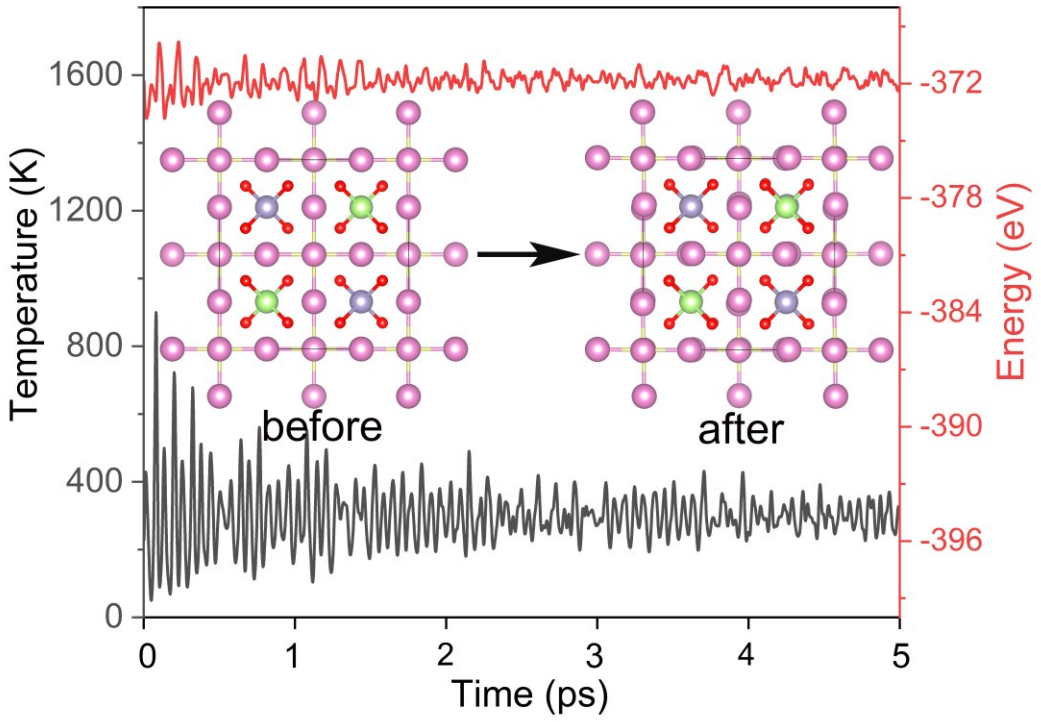

Figure S3. Fluctuations of total energy (red) and temperature T (black) during AIMD (ab initio molecular dynamics) simulations at 300 K. Insets show the crystal structures of $IrIn_6GaSnO_8$ at 0 and 5 ps of AIMD simulations. The golden, violet, pale green, light gray, and red balls represent the Ir, In, Ga, Sn, and O atoms, respectively.

4. Variation of energy and temperature against time for the AIMD simulation of $IrIn_6GaTiO_8$

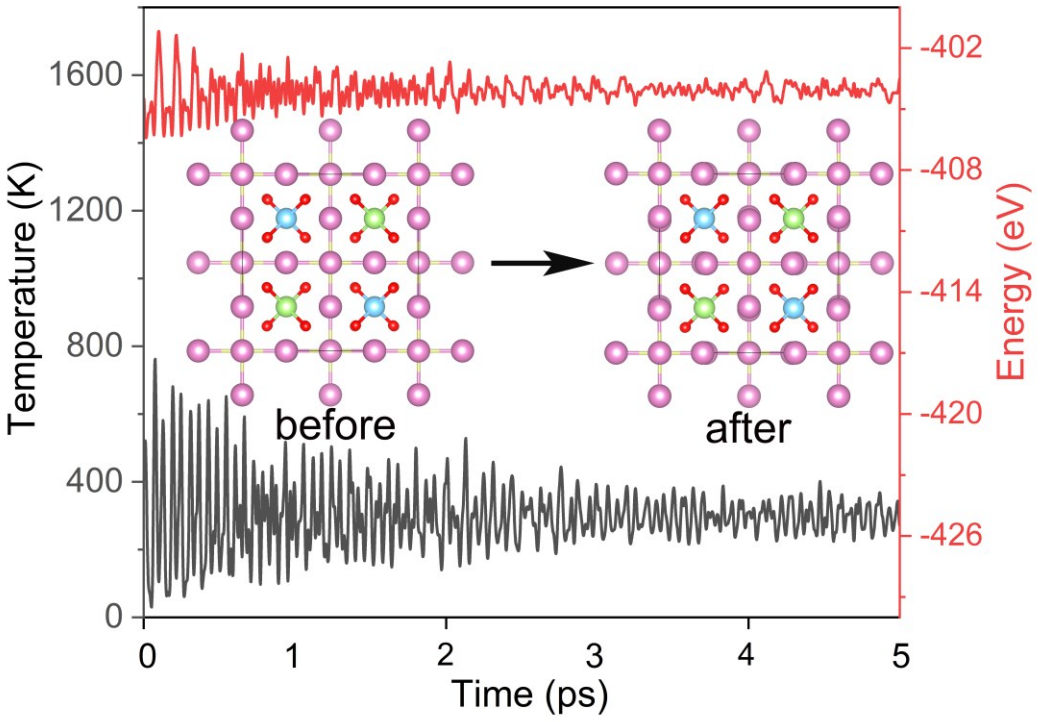

Figure S4. Fluctuations of total energy (red) and temperature T (black) during AIMD (ab initio molecular dynamics) simulations at 300 K. Insets show the crystal structures of $IrIn_6GaTiO_8$ at 0 and 5 ps of AIMD simulations. The golden, violet, pale green, sky blue, and red balls represent the Ir, In, Ga, Ti, and O atoms, respectively.

5. Variation of energy and temperature against time for the AIMD simulation of $IrIn_6InGeO_8$

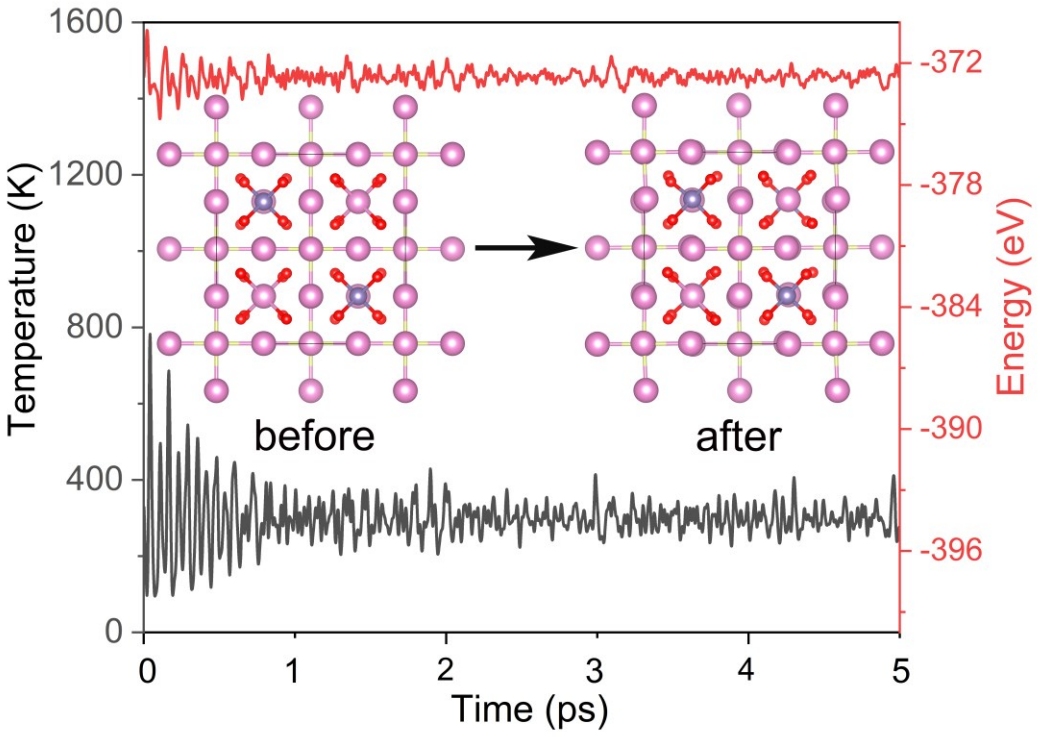

Figure S5. Fluctuations of total energy (red) and temperature T (black) during AIMD (ab initio molecular dynamics) simulations at 300 K. Insets show the crystal structures of $IrIn_6InGeO_8$ at 0 and 5 ps of AIMD simulations. The golden, violet, gray, and red balls represent the Ir, In, Ge, and O atoms, respectively.

6. Variation of energy and temperature against time for the AIMD simulation of $IrIn_6InSnO_8$

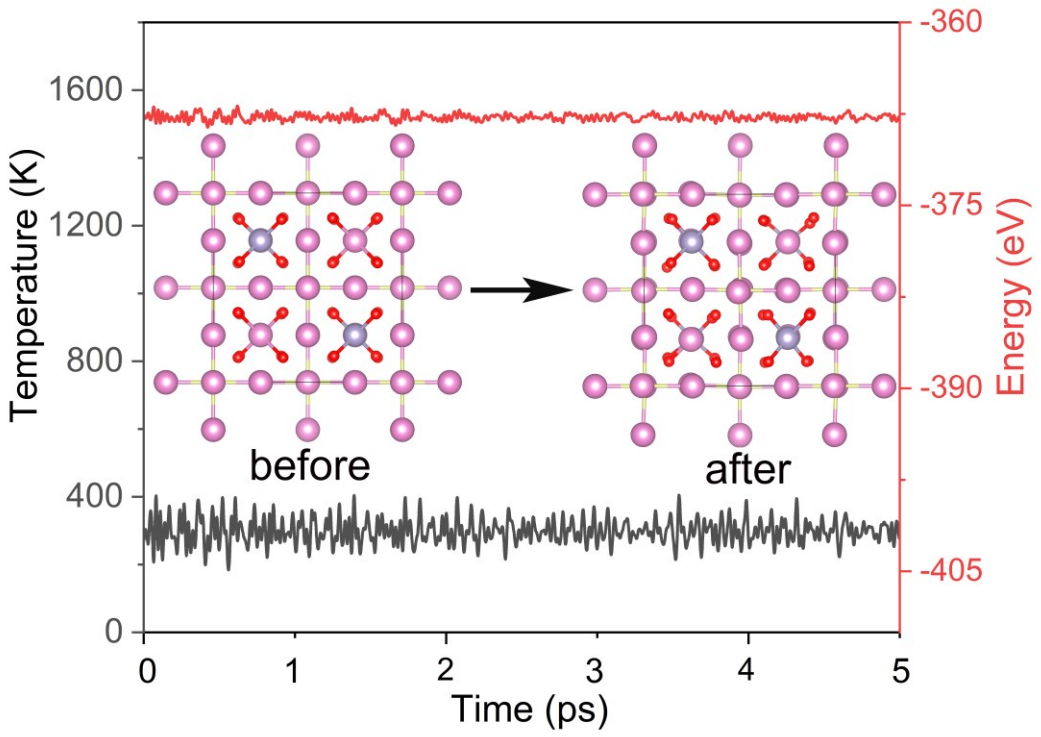

Figure S6. Fluctuations of total energy (red) and temperature T (black) during AIMD (ab initio molecular dynamics) simulations at 300 K. Insets show the crystal structures of $IrIn_6InSnO_8$ at 0 and 5 ps of AIMD simulations. The golden, violet, light gray, and red balls represent the Ir, In, Sn, and O atoms, respectively.

7. Variation of energy and temperature against time for the AIMD simulation of $IrIn_6InTiO_8$

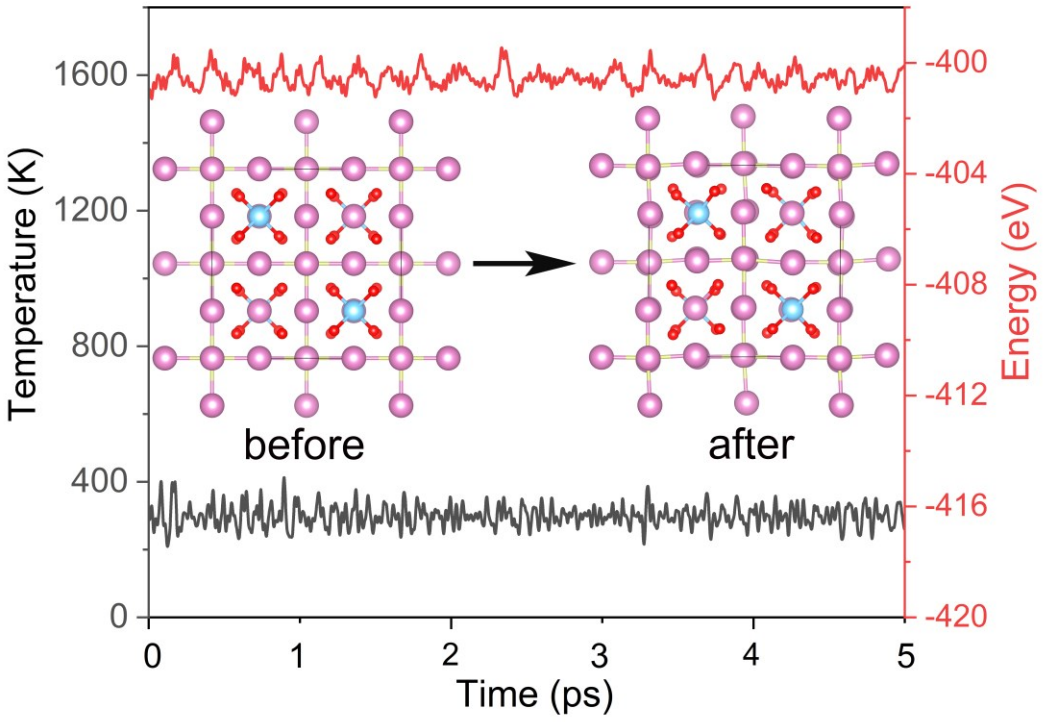

Figure S7. Fluctuations of total energy (red) and temperature T (black) during AIMD (ab initio molecular dynamics) simulations at 300 K. Insets show the crystal structures of $IrIn_6InTiO_8$ at 0 and 5 ps of AIMD simulations. The golden, violet, sky blue, and red balls represent the Ir, In, Ti, and O atoms, respectively.

8. Fatband Structures of $IrIn_6GaGeO_8$

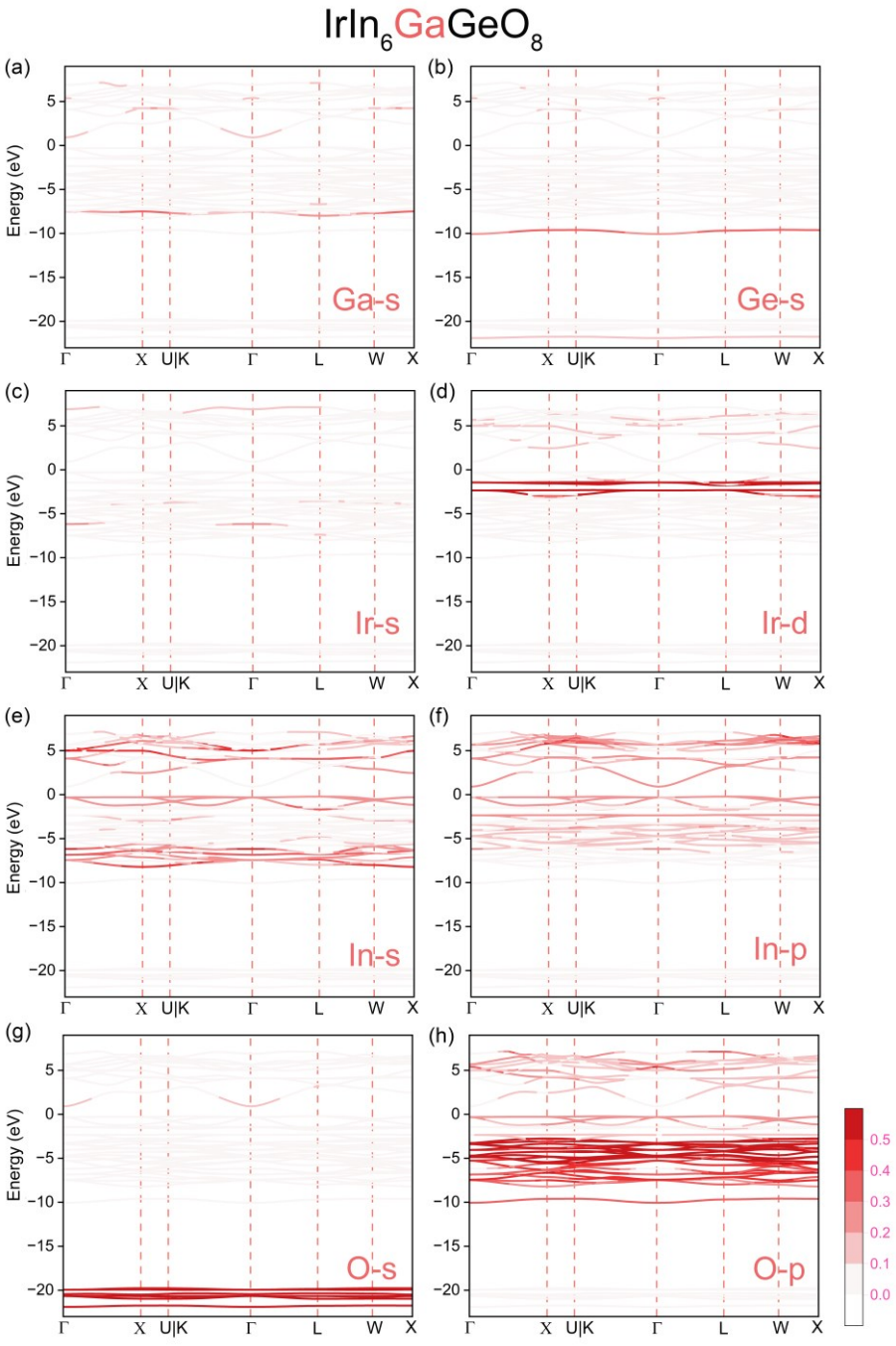

Figure S8. Atomic orbital projections for $IrIn_6GaGeO_8$ showing the relative contribution of each atomic orbital, which was calculated using DFT with the HSE06 functional. The color and thickness of the bands indicates the percentage of orbital character, where red denoting a greater contribution.

9. Fatband Structures of $IrIn_6GaSnO_8$

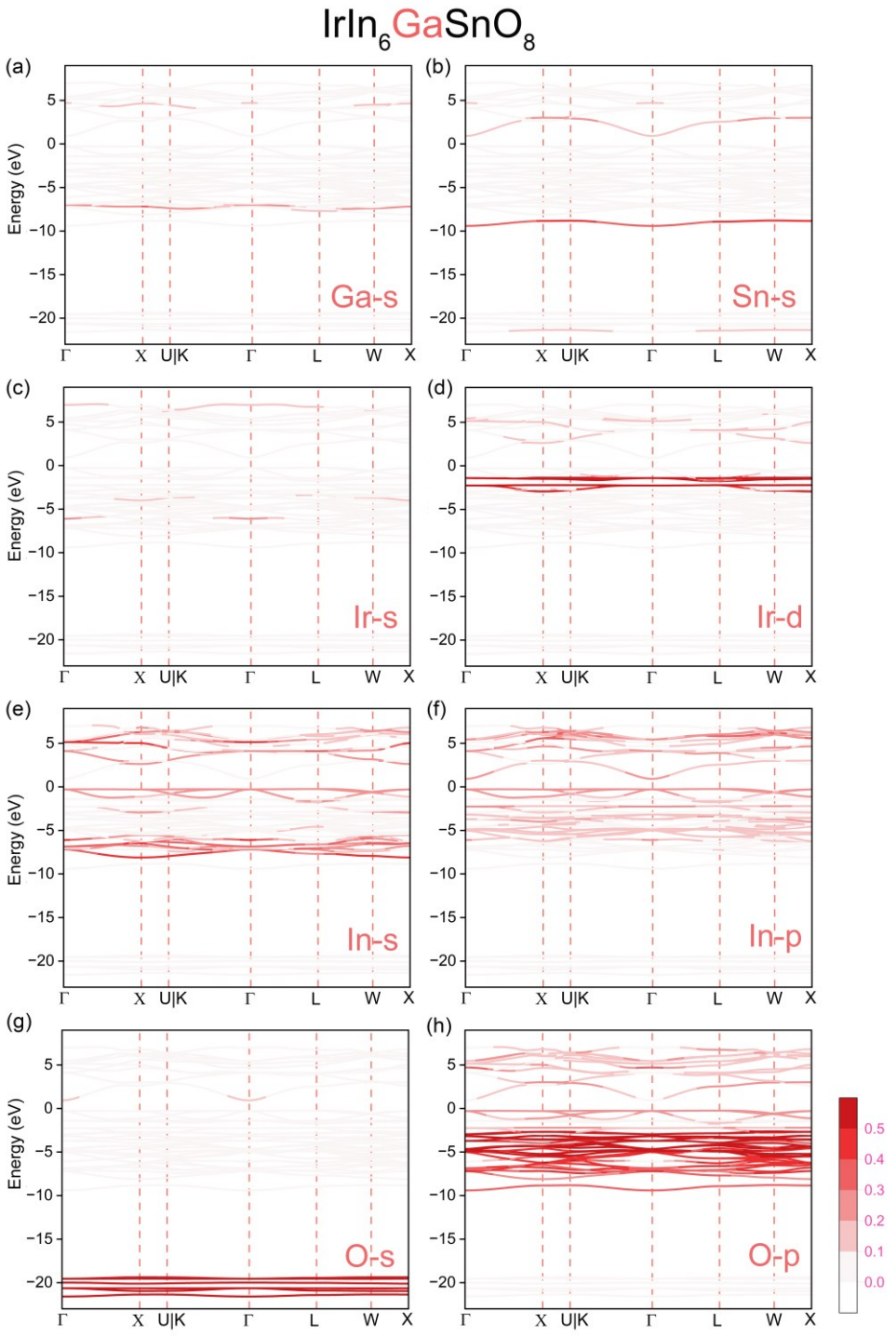

Figure S9. Atomic orbital projections for $IrIn_6GaSnO_8$ showing the relative contribution of each atomic orbital, which was calculated using DFT with the HSE06 functional.

10. Fatband Structures of $IrIn_6GaTiO_8$

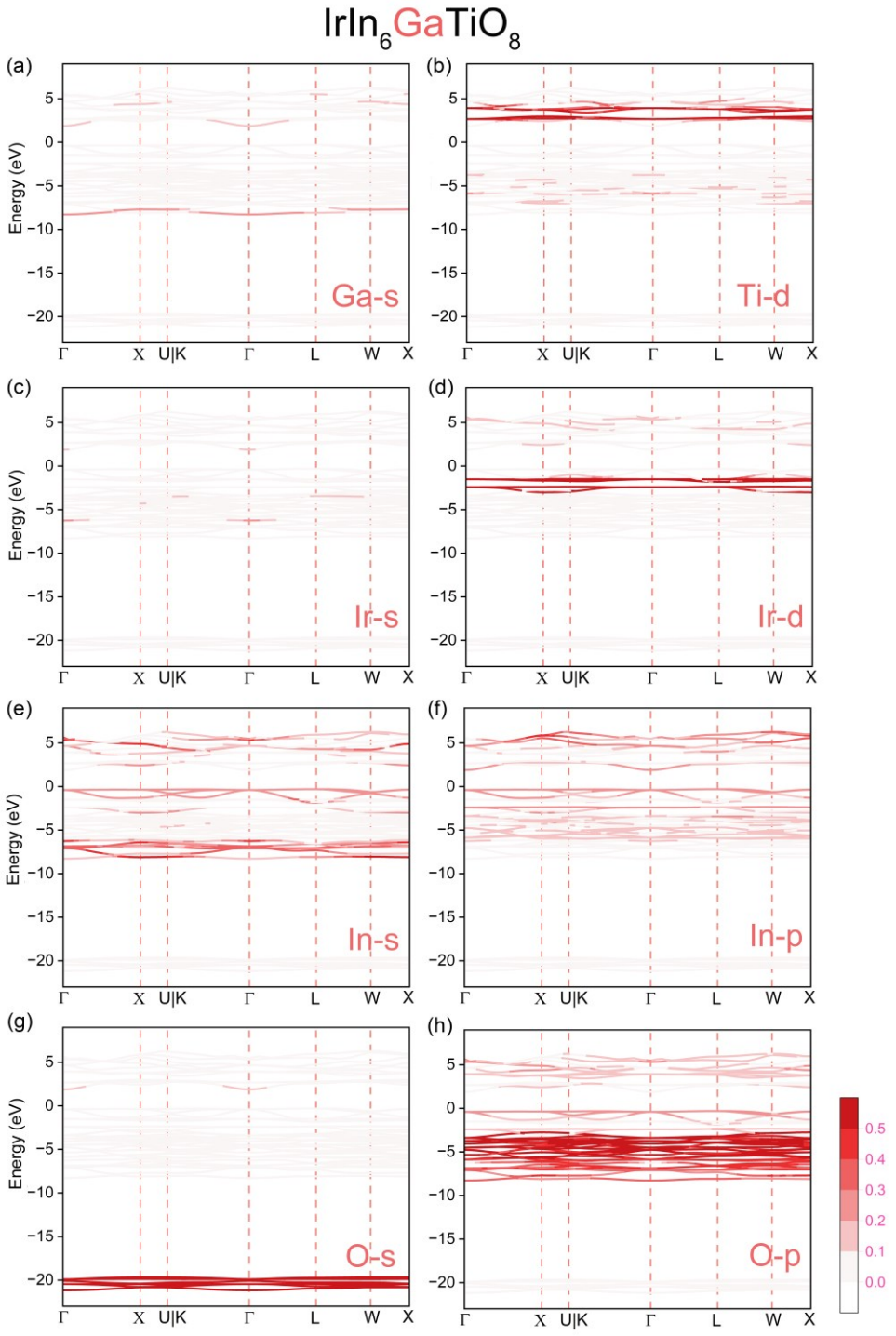

Figure S10. Atomic orbital projections for $IrIn_6GaTiO_8$ showing the relative contribution of each atomic orbital, which was calculated using DFT with the HSE06 functional.

11. Fatband Structures of $IrIn_6InGeO_8$

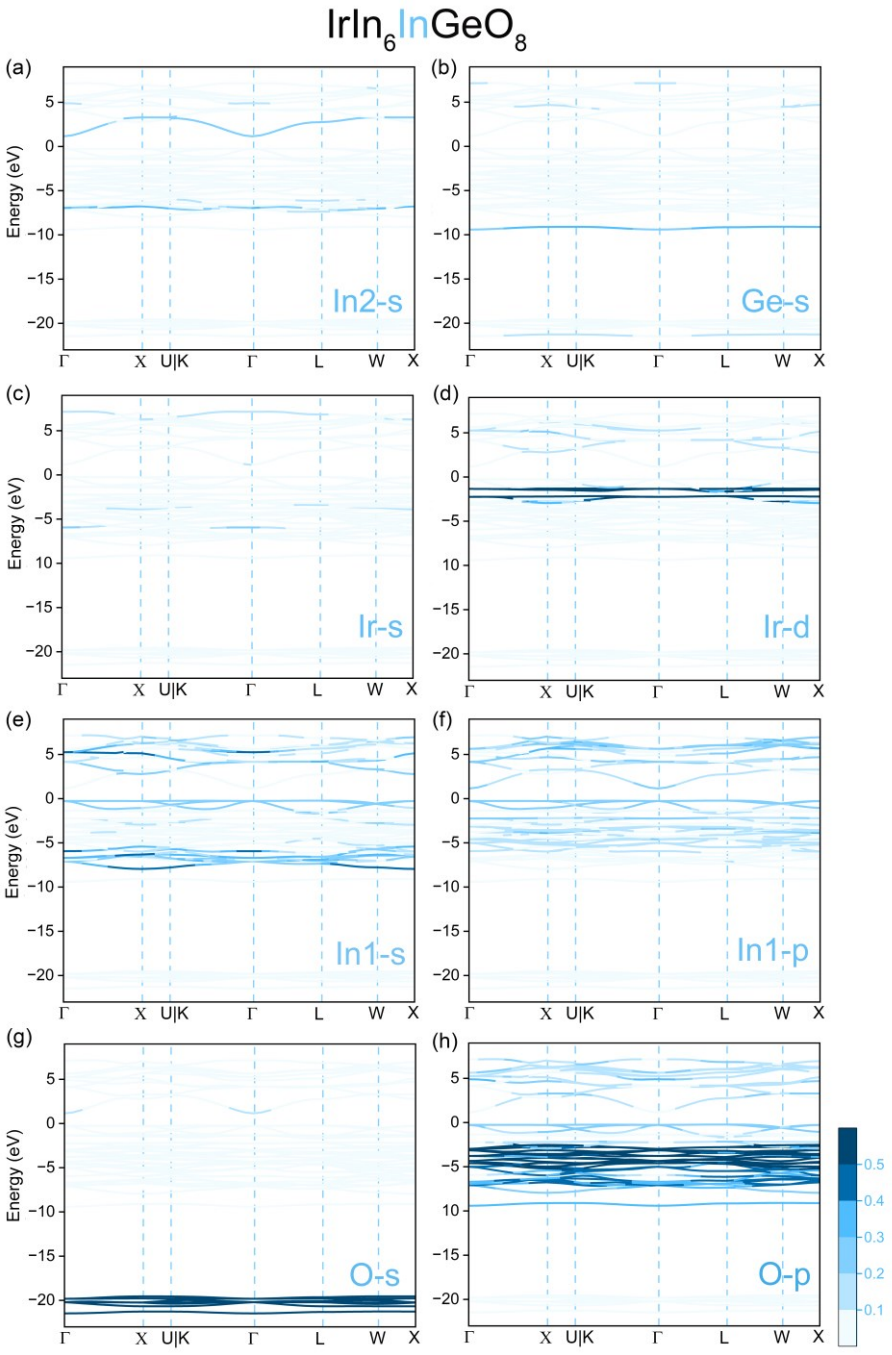

Figure S11. Atomic orbital projections for $IrIn_6InGeO_8$ showing the relative contribution of each atomic orbital, which was calculated using DFT with the HSE06 functional. The color and thickness of the bands indicates the percentage of orbital character, where blue denoting a greater contribution.

12. Fatband Structures of $IrIn_6InSnO_8$

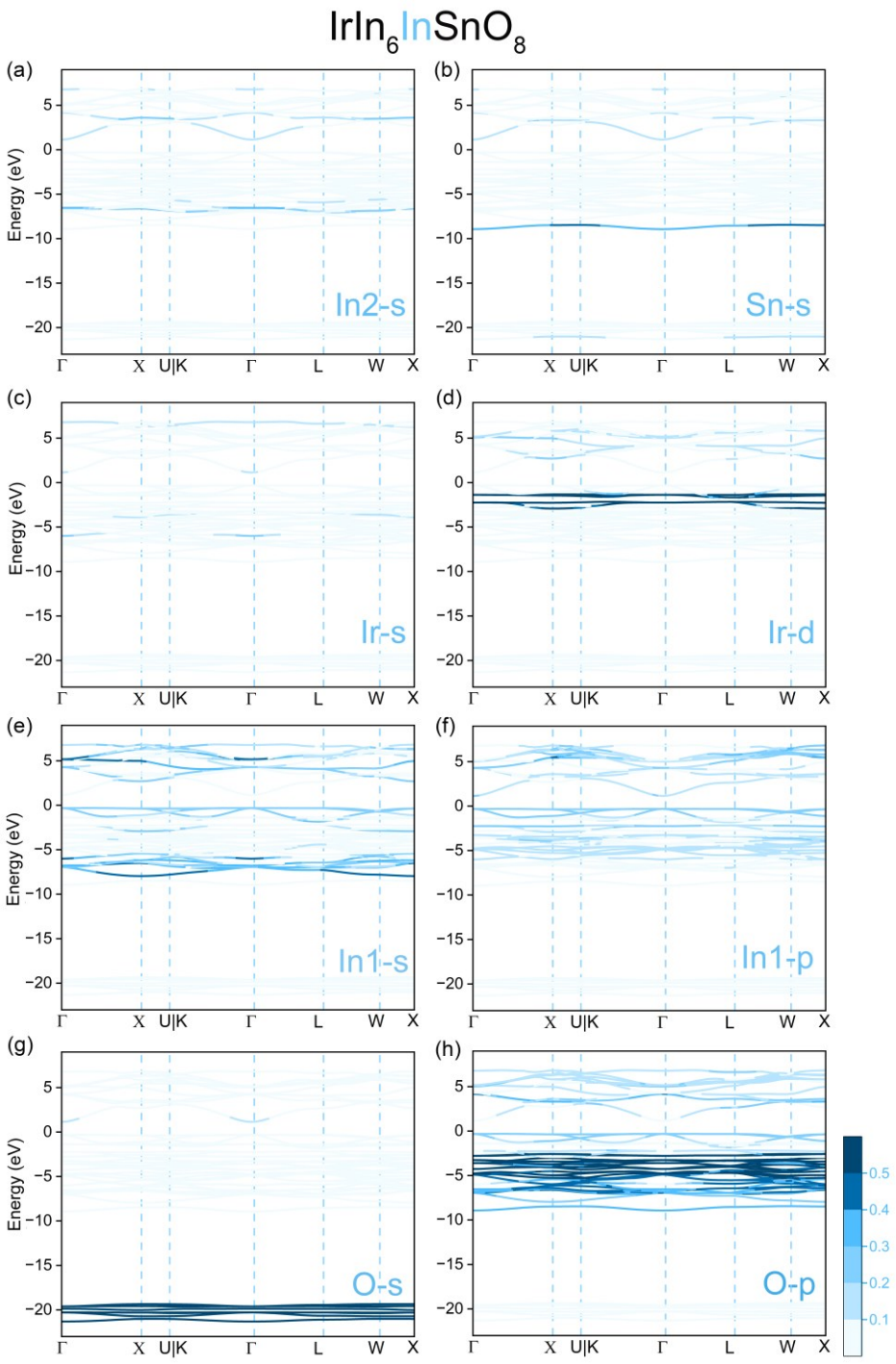

Figure S12. Atomic orbital projections for $IrIn_6InSnO_8$ showing the relative contribution of each atomic orbital, which was calculated using DFT with the HSE06 functional.

13. Fatband Structures of $IrIn_6InTiO_8$

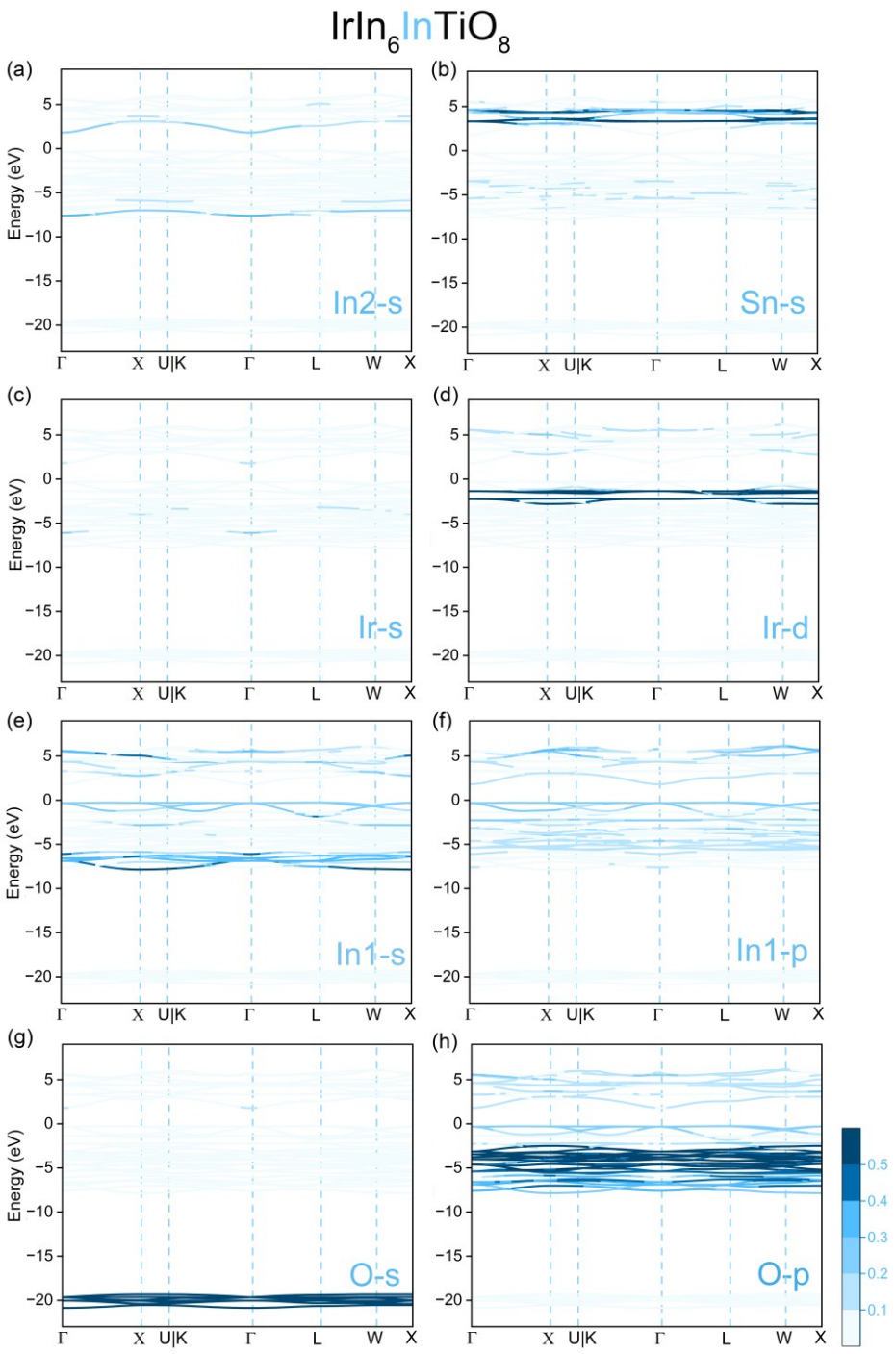

Figure S13. Atomic orbital projections for $IrIn_6InTiO_8$ showing the relative contribution of each atomic orbital, which was calculated using DFT with the HSE06 functional.

14. DOS of $IrIn_6XYO_8$ (*X*=Ga, In; *Y*=Ge, Sn, Ti)

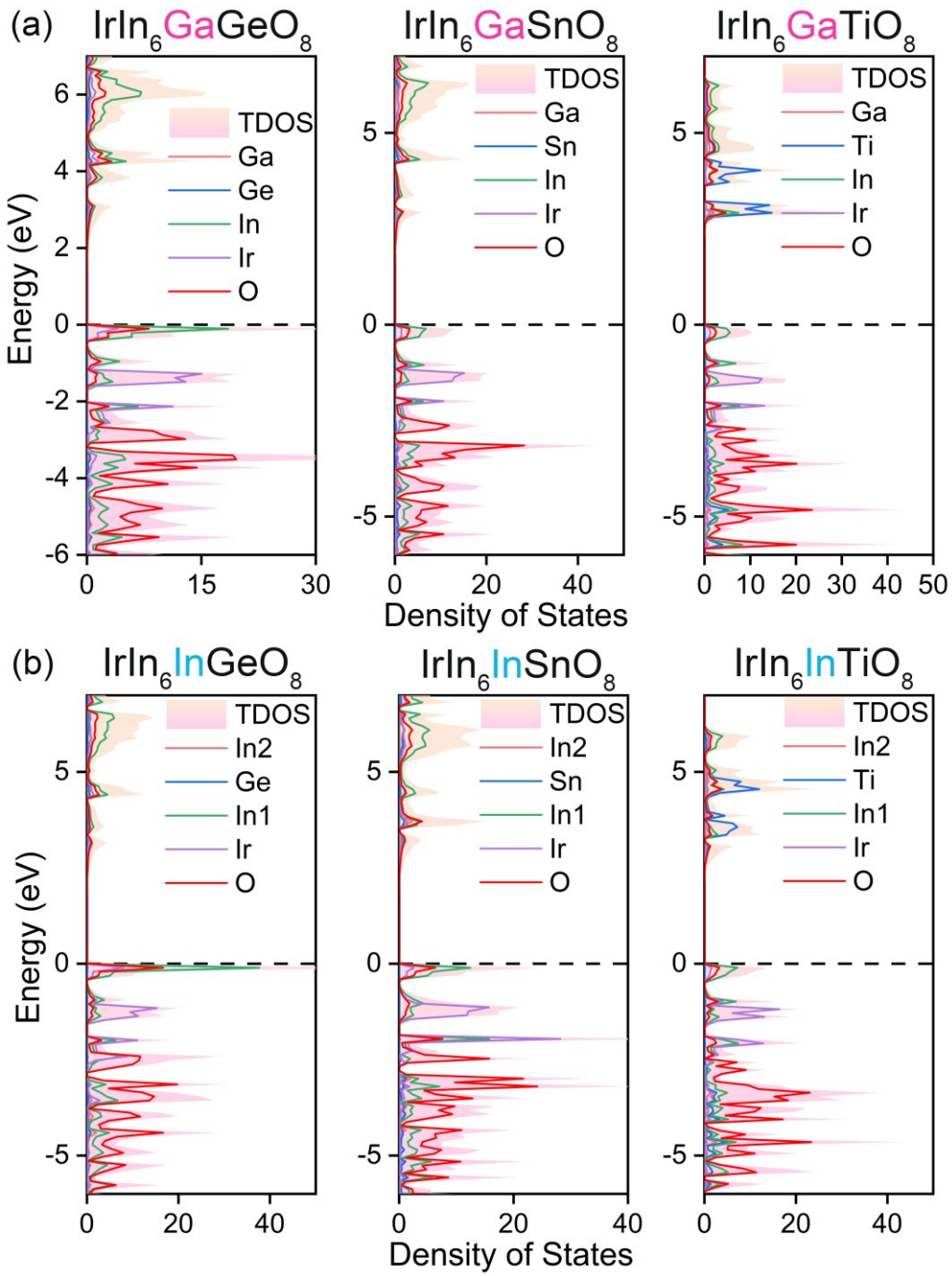

Figure S14. Calculated DOS (density of states) of $IrIn_6XYO_8$ (*X*=Ga, In; *Y*=Ge, Sn, Ti).

15. Partial DOS of $IrIn_6GaGeO_8$

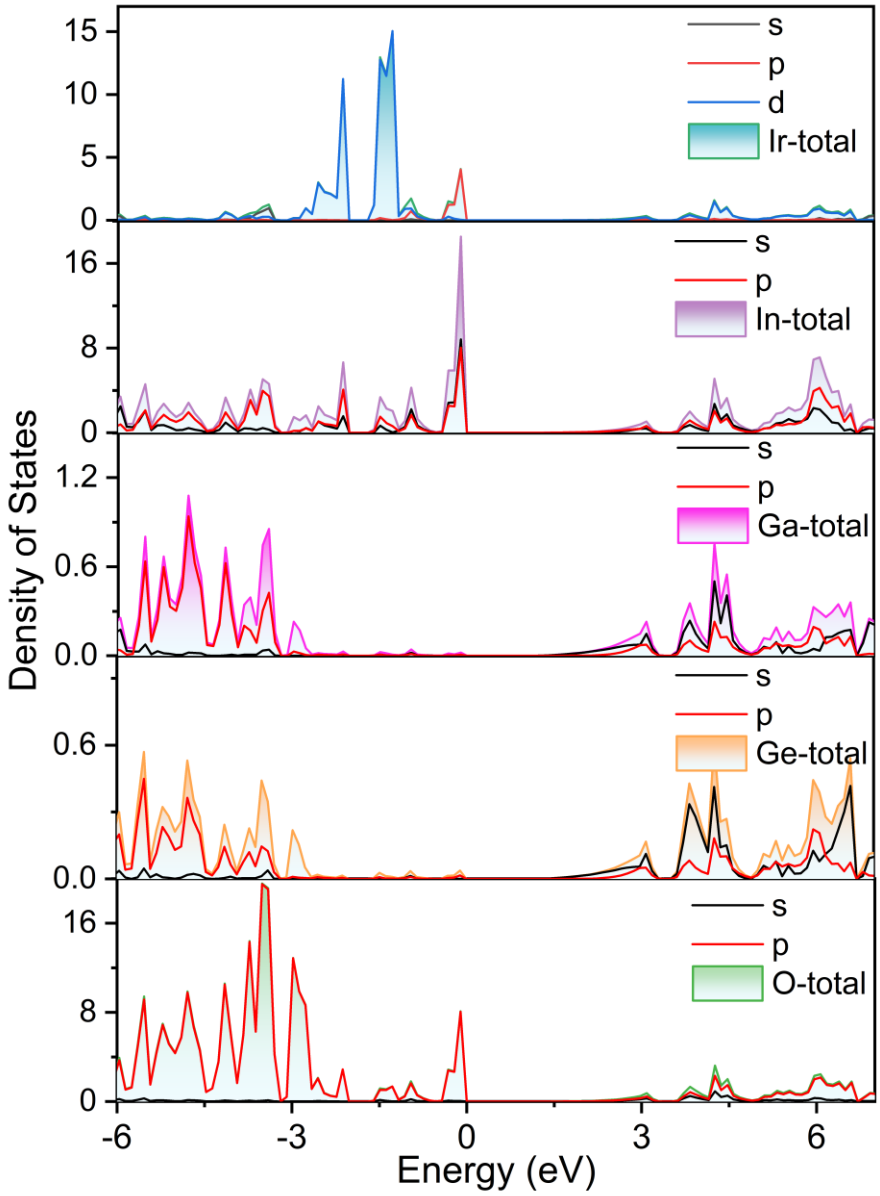

Figure S15. Calculated PDOS (partial density of states) of $IrIn_6GaGeO_8$.

16. Partial DOS of $IrIn_6GaSnO_8$

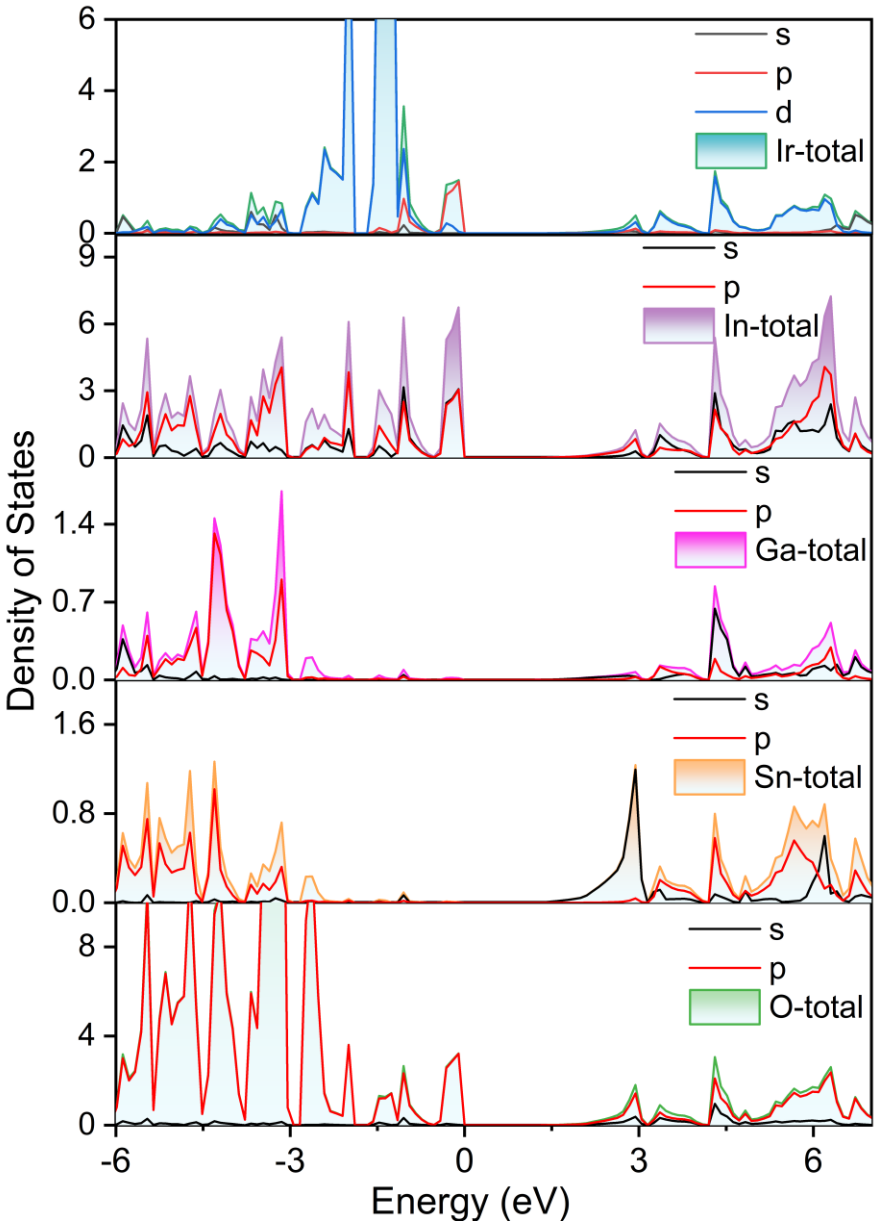

Figure S16. Calculated PDOS (partial density of states) of $IrIn_6GaSnO_8$.

17. Partial DOS of $IrIn_6GaTiO_8$

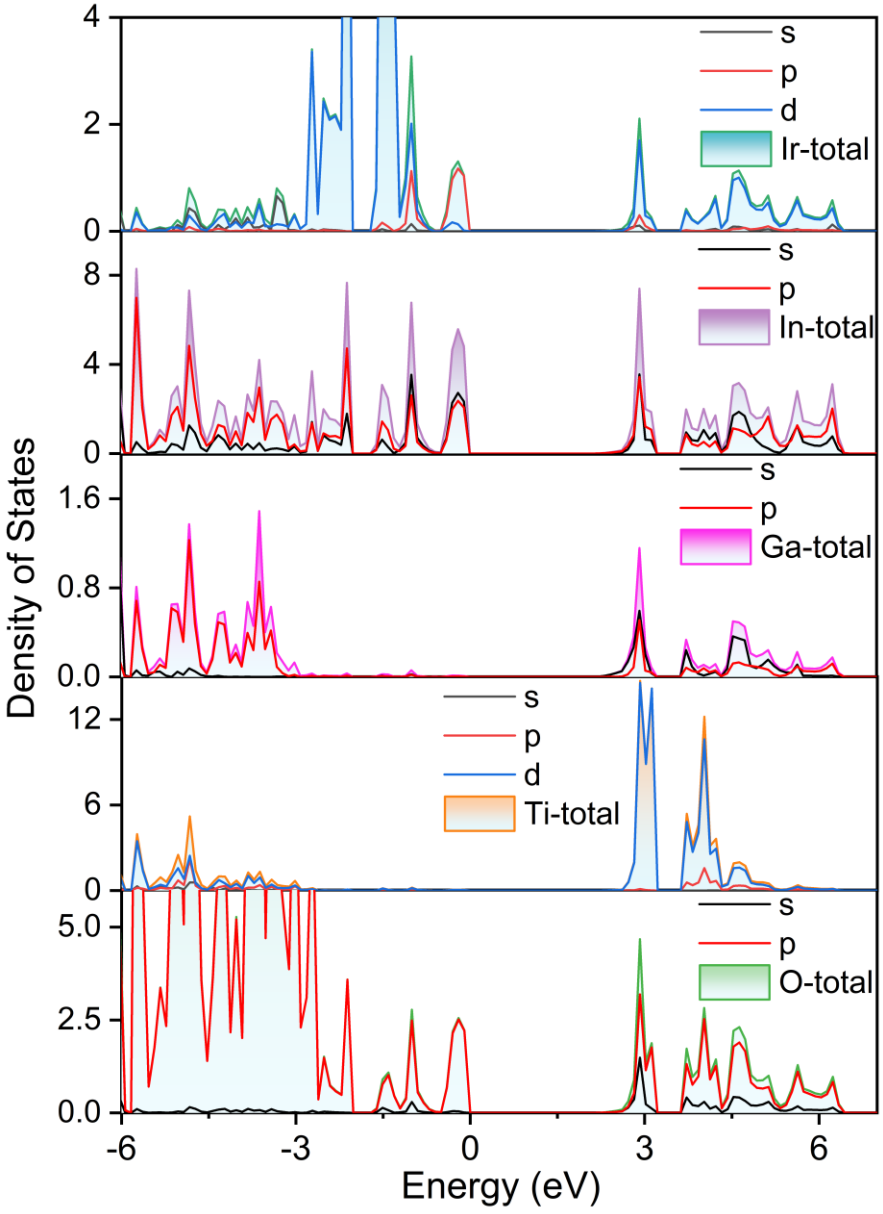

Figure S17. Calculated PDOS (partial density of states) of $IrIn_6GaTiO_8$.

18. Partial DOS of $IrIn_6InGeO_8$

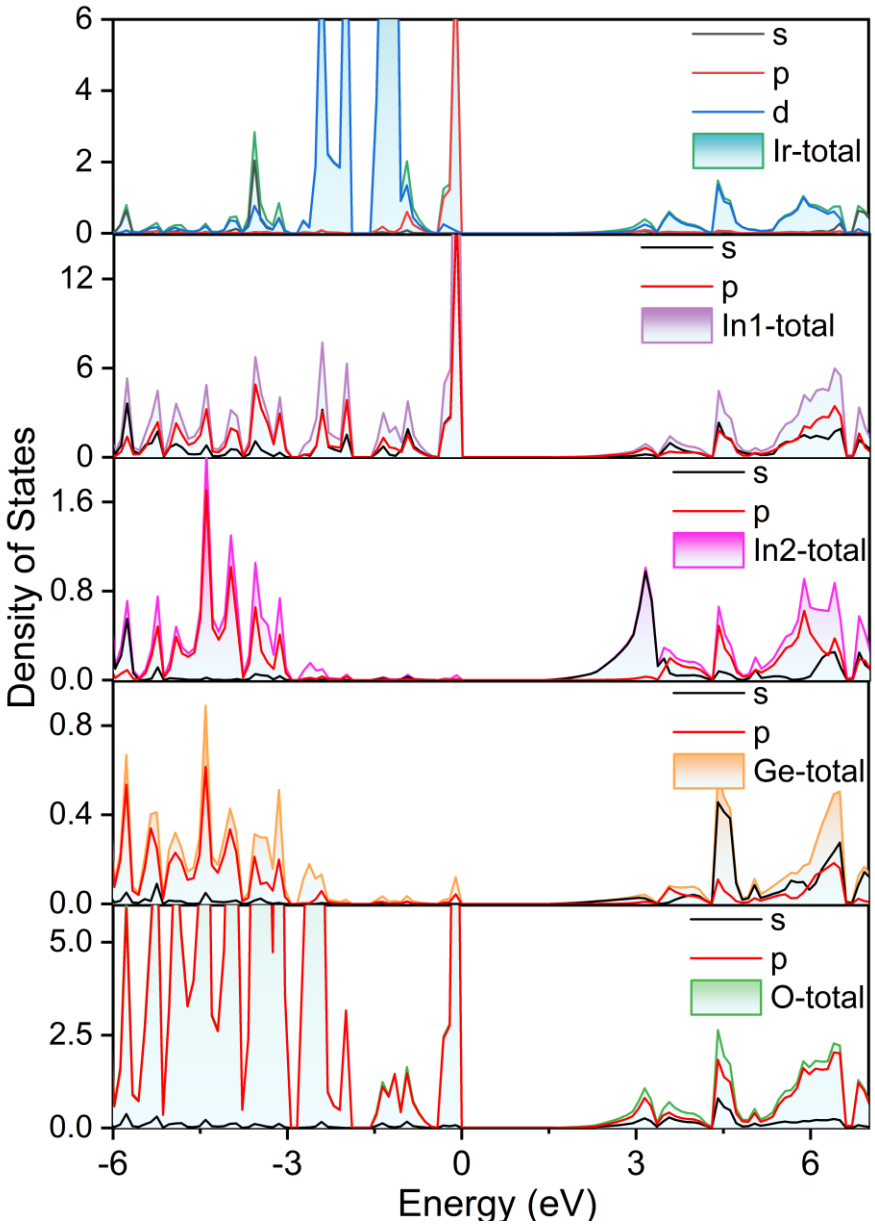

Figure S18. Calculated PDOS (partial density of states) of $IrIn_6InGeO_8$.

19. Partial DOS of $IrIn_6InSnO_8$

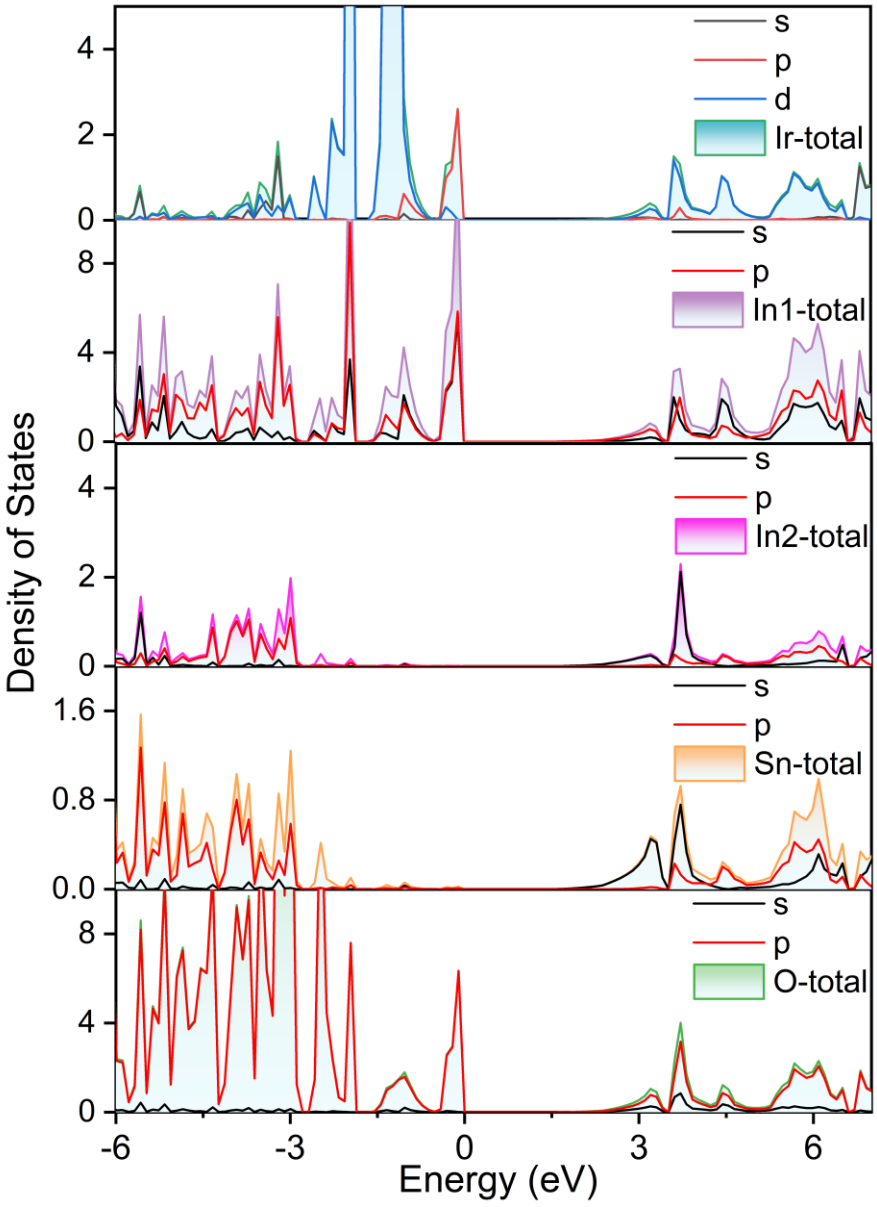

Figure S19. Calculated PDOS (partial density of states) of $IrIn_6InSnO_8$.

20. Partial DOS of $IrIn_6InTiO_8$

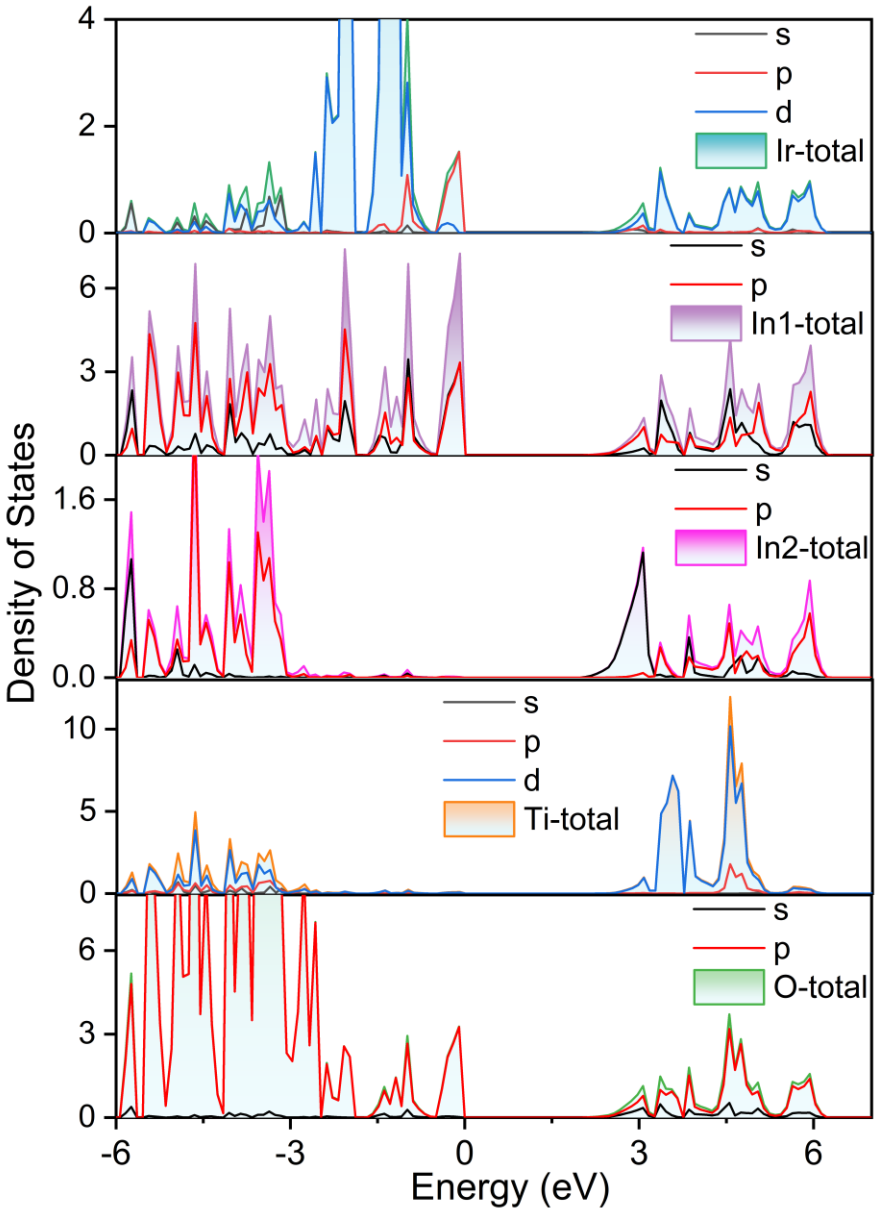

Figure S20. Calculated PDOS (partial density of states) of $IrIn_6InTiO_8$.

21. 1D ELF profile and 2D ELF isosurface for $IrIn_6GaGeO_8$

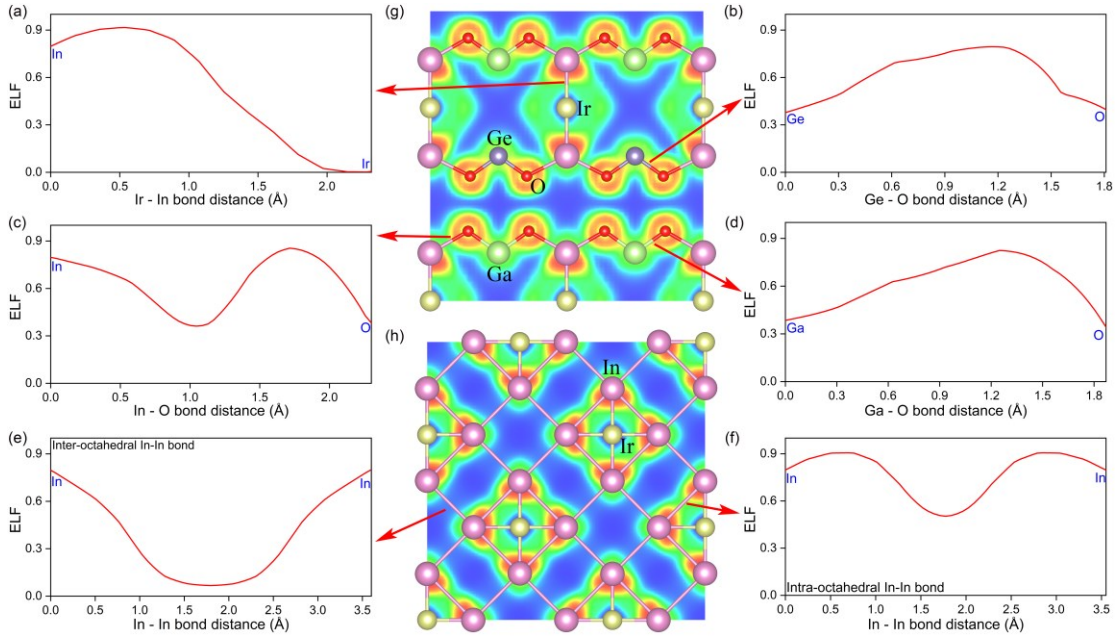

Figure S21. 1D ELF profile analyzed for the (a) Ir-In, (b) Ge-O, (c) In-O, (d) Ga-O, (e) inter-octahedral In-In and (f) intra-octahedral In-In bonds in $IrIn_6GaGeO_8$. The plot in (g) and (h) depict 2D ELF isosurface, which are sliced perpendicular in the (100) and (101) directions, respectively.

22. 1D ELF profile and 2D ELF isosurface for $IrIn_6GaSnO_8$

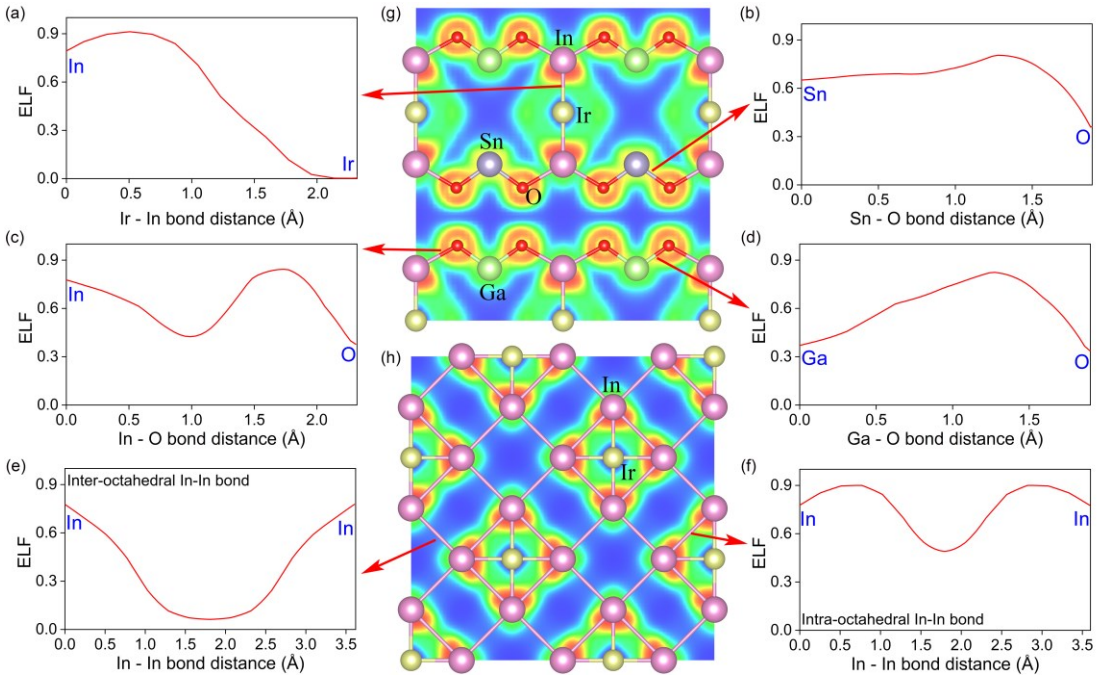

Figure S22. 1D ELF profile analyzed for the (a) Ir-In, (b) Sn-O, (c) In-O, (d) Ga-O, (e) inter-octahedral In-In and (f) intra-octahedral In-In bonds in $IrIn_6GaSnO_8$. The plot in (g) and (h) depict 2D ELF isosurface, which are sliced perpendicular in the (100) and (101) directions, respectively.

23. 1D ELF profile and 2D ELF isosurface for $IrIn_6GaTiO_8$

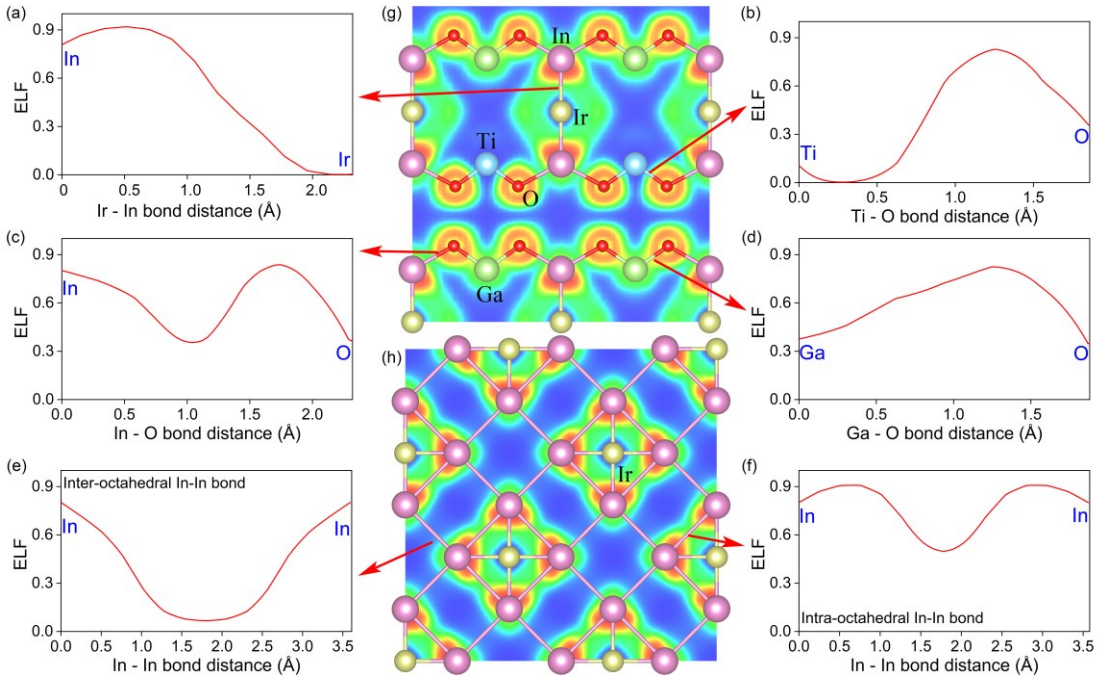

Figure S23. 1D ELF profile analyzed for the (a) Ir-In, (b) Ti-O, (c) In-O, (d) Ga-O, (e) inter-octahedral In-In and (f) intra-octahedral In-In bonds in $IrIn_6GaTiO_8$. The plot in (g) and (h) depict 2D ELF isosurface, which are sliced perpendicular in the (100) and (101) directions, respectively.

24. 1D ELF profile and 2D ELF isosurface for $IrIn_{(1)6}In_{(2)}GeO_8$

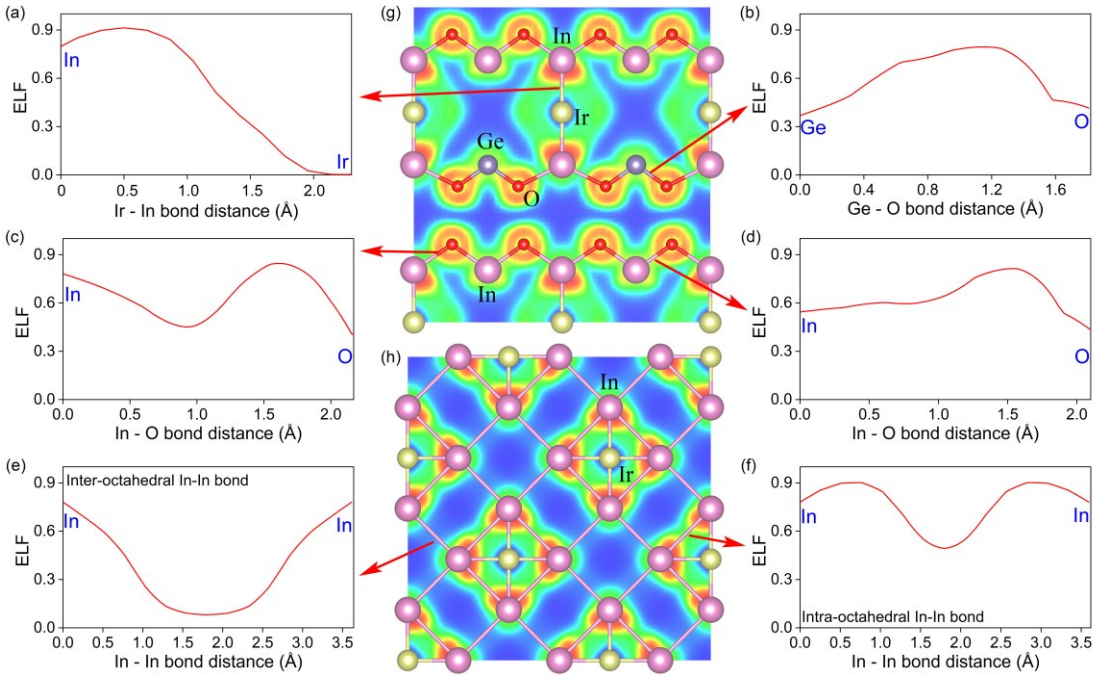

Figure S24. 1D ELF profile analyzed for the (a) Ir-In, (b) Ge-O, (c) In1-O, (d) In2-O, (e) inter-octahedral In-In and (f) intra-octahedral In-In bonds in $IrIn_{(1)6}In_{(2)}GeO_8$. The plot in (g) and (h) depict 2D ELF isosurface, which are sliced perpendicular in the (100) and (101) directions, respectively.

25. 1D ELF profile and 2D ELF isosurface for $IrIn_{(1)6}In_{(2)}SnO_8$

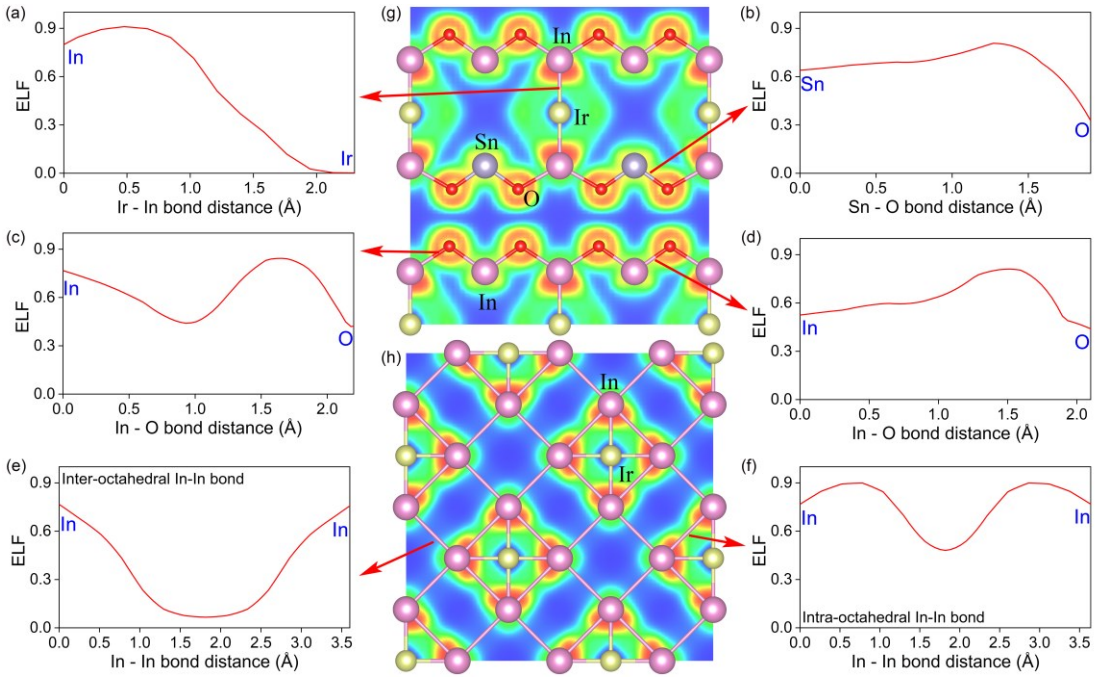

Figure S25. 1D ELF profile analyzed for the (a) Ir-In, (b) Sn-O, (c) In-1O, (d) In2-O, (e) inter-octahedral In-In and (f) intra-octahedral In-In bonds in $IrIn_{(1)6}In_{(2)}SnO_8$. The plot in (g) and (h) depict 2D ELF isosurface, which are sliced perpendicular in the (100) and (101) directions, respectively.

26. 1D ELF profile and 2D ELF isosurface for $IrIn_{(1)6}In_{(2)}TiO_8$

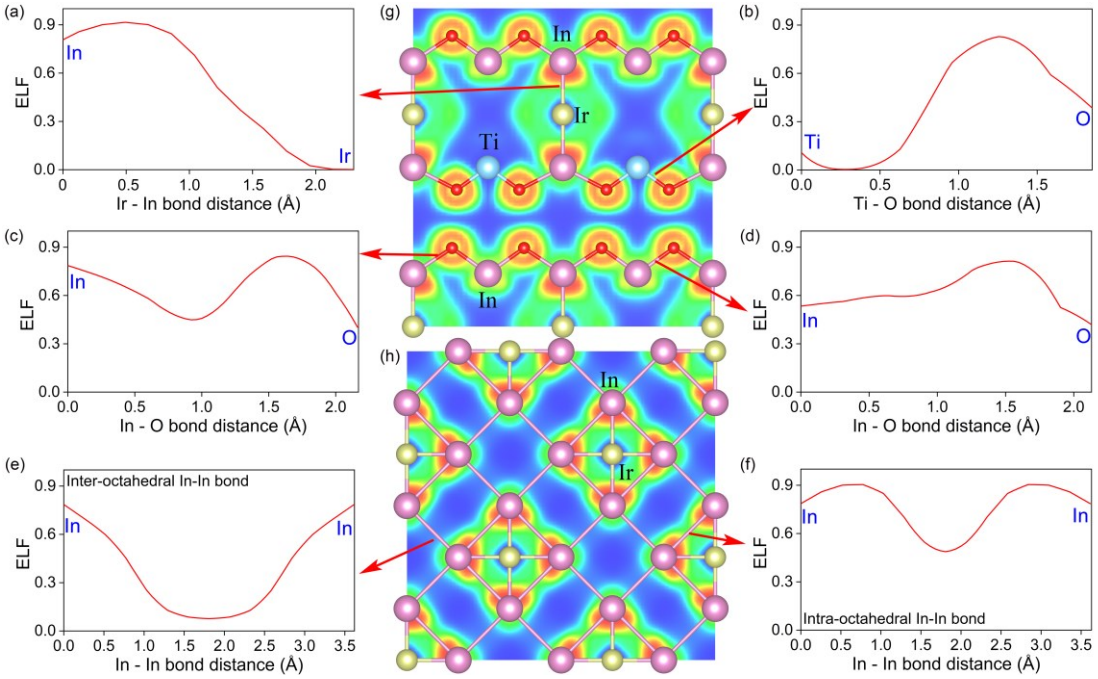

Figure S26. 1D ELF profile analyzed for the (a) Ir-In, (b) Ti-O, (c) In1-O, (d) In2-O, (e) inter-octahedral In-In and (f) intra-octahedral In-In bonds in $IrIn_{(1)6}In_{(2)}TiO_8$. The plot in (g) and (h) depict 2D ELF isosurface, which are sliced perpendicular in the (100) and (101) directions, respectively.

27. pCOHP and pCOBI of $IrIn_6GaGeO_8$

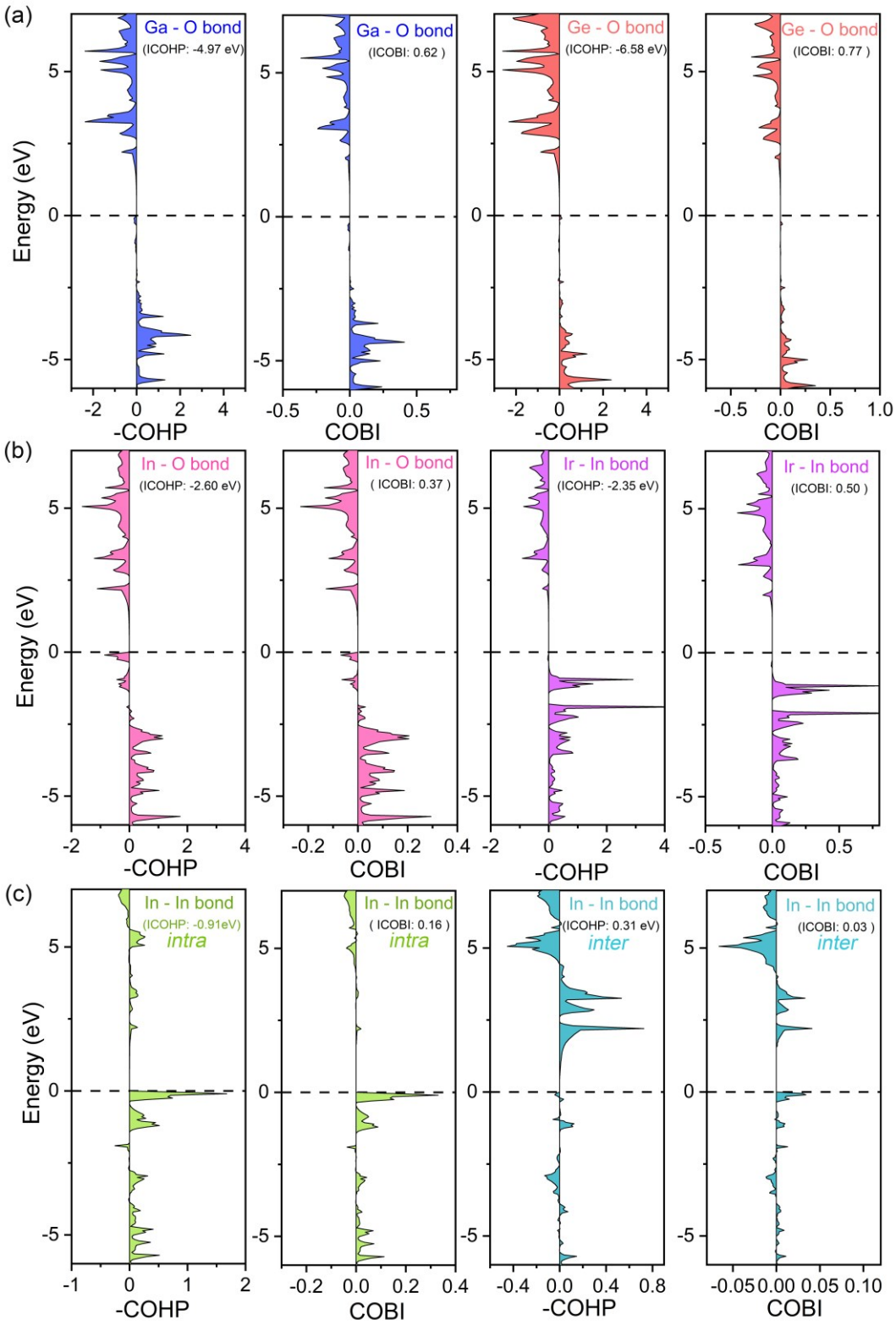

Figure S27. Calculated pCOHP (partial crystal orbital Hamilton population) and pCOBI (partial crystal orbital bond indices) of $IrIn_6GaGeO_8$.

28. pCOHP and pCOBI of $IrIn_6GaSnO_8$

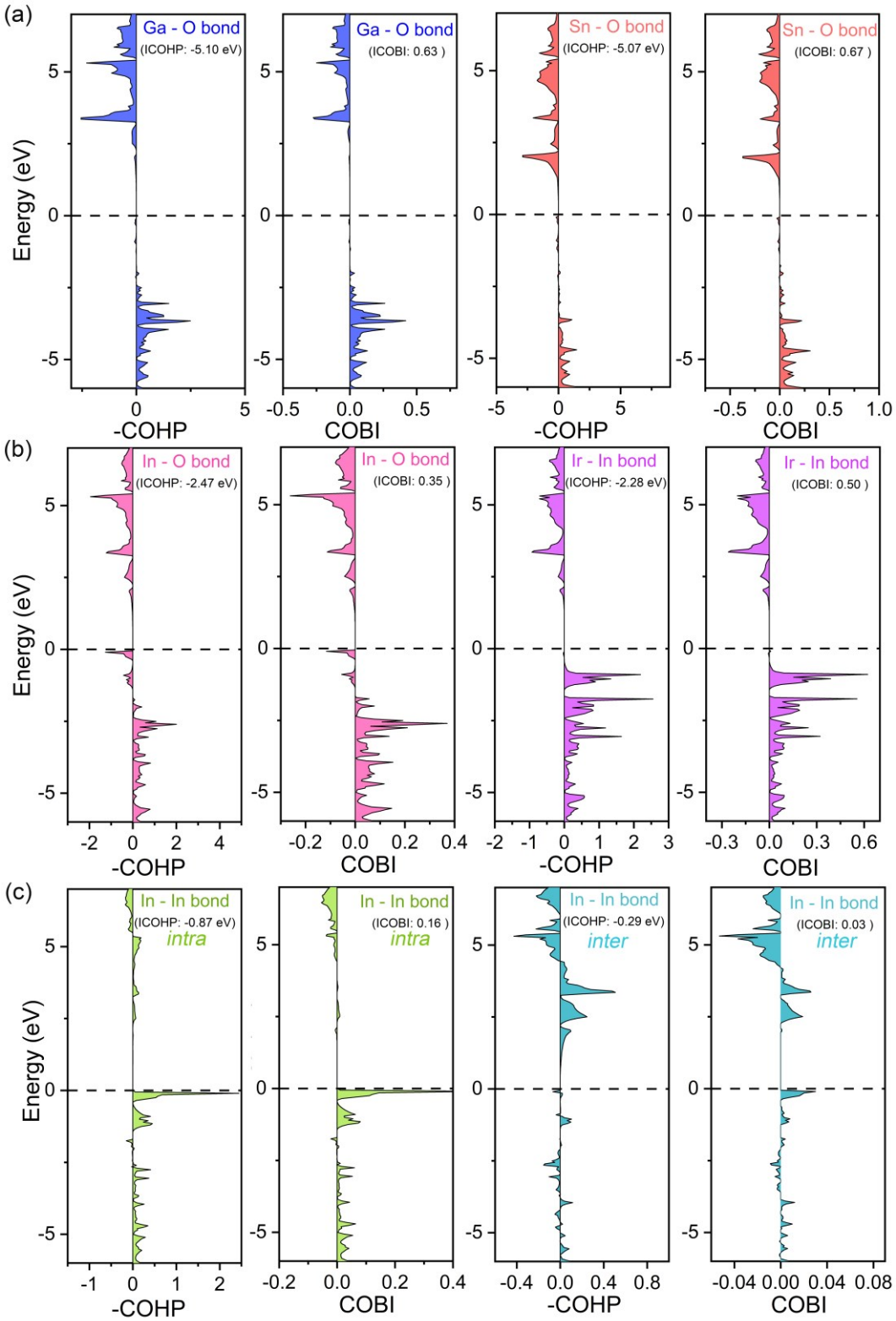

Figure S28. Calculated pCOHP (partial crystal orbital Hamilton population) and pCOBI (partial crystal orbital bond indices) of $IrIn_6GaSnO_8$.

29. pCOHP and pCOBI of $IrIn_6GaTiO_8$

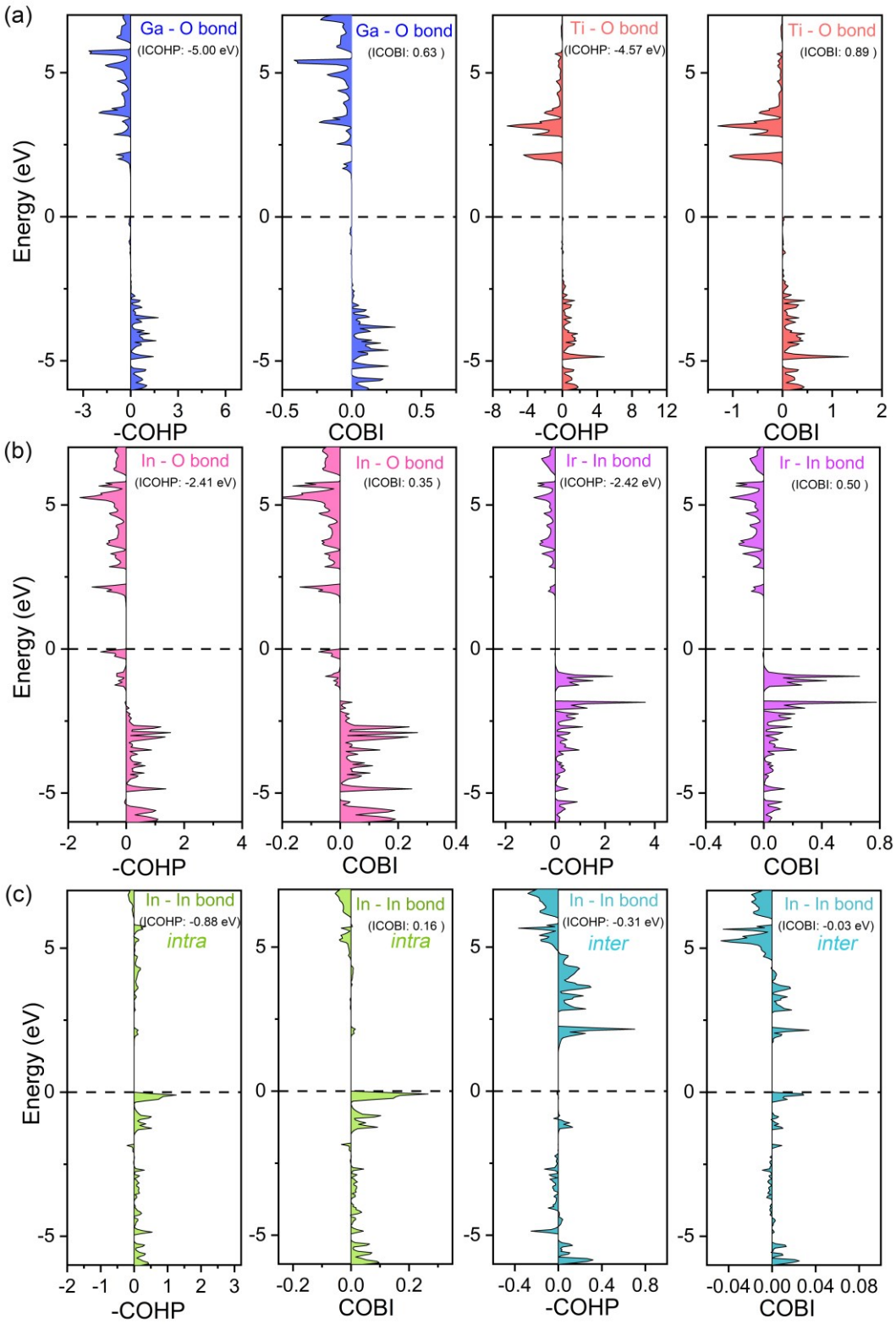

Figure S29. Calculated pCOHP (partial crystal orbital Hamilton population) and pCOBI (partial crystal orbital bond indices) of $IrIn_6GaTiO_8$.

30. pCOHP and pCOBI of $IrIn_6InGeO_8$

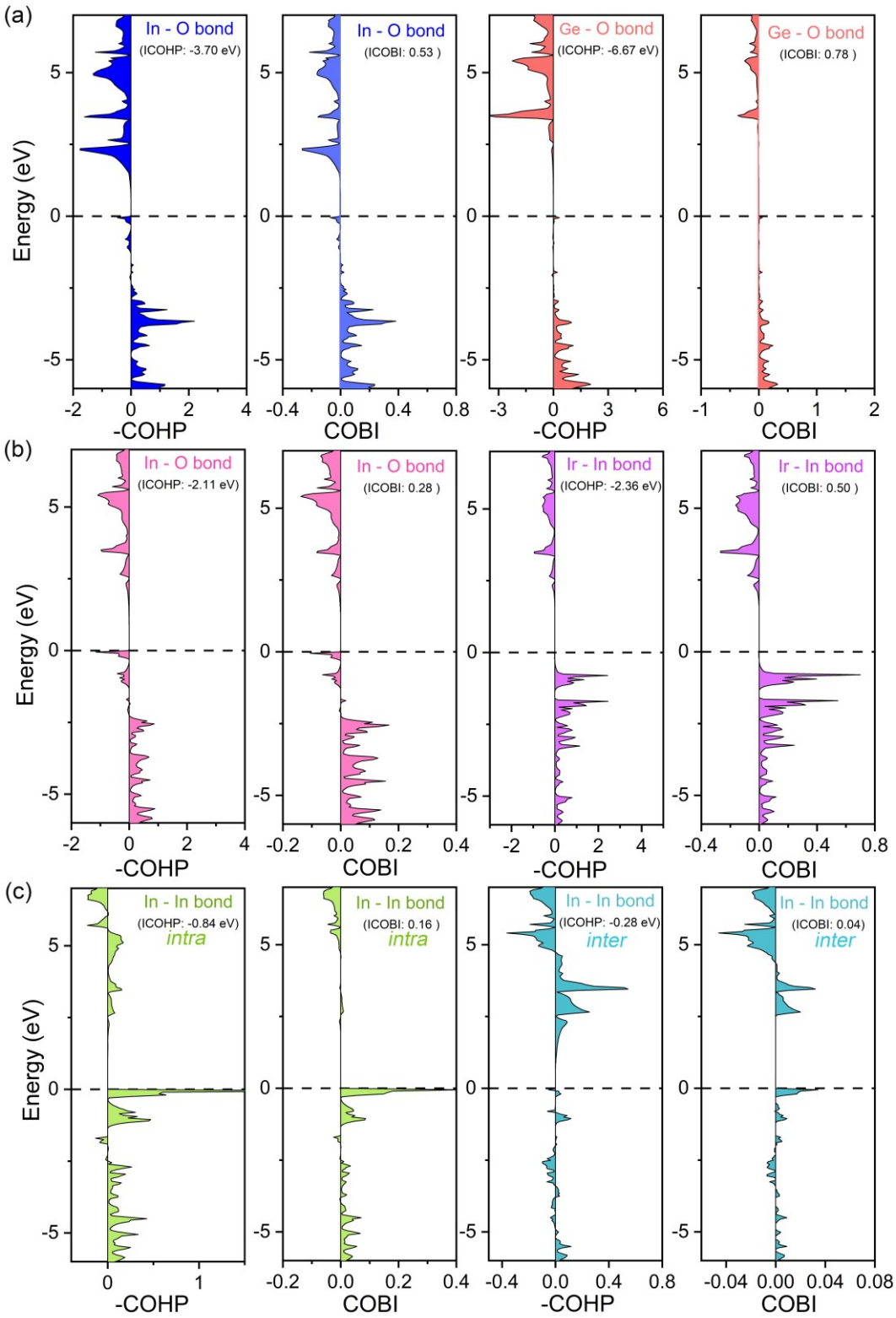

Figure S30. Calculated pCOHP (partial crystal orbital Hamilton population) and pCOBI (partial crystal orbital bond indices) of $IrIn_6InGeO_8$.

31. pCOHP and pCOBI of $IrIn_6InSnO_8$

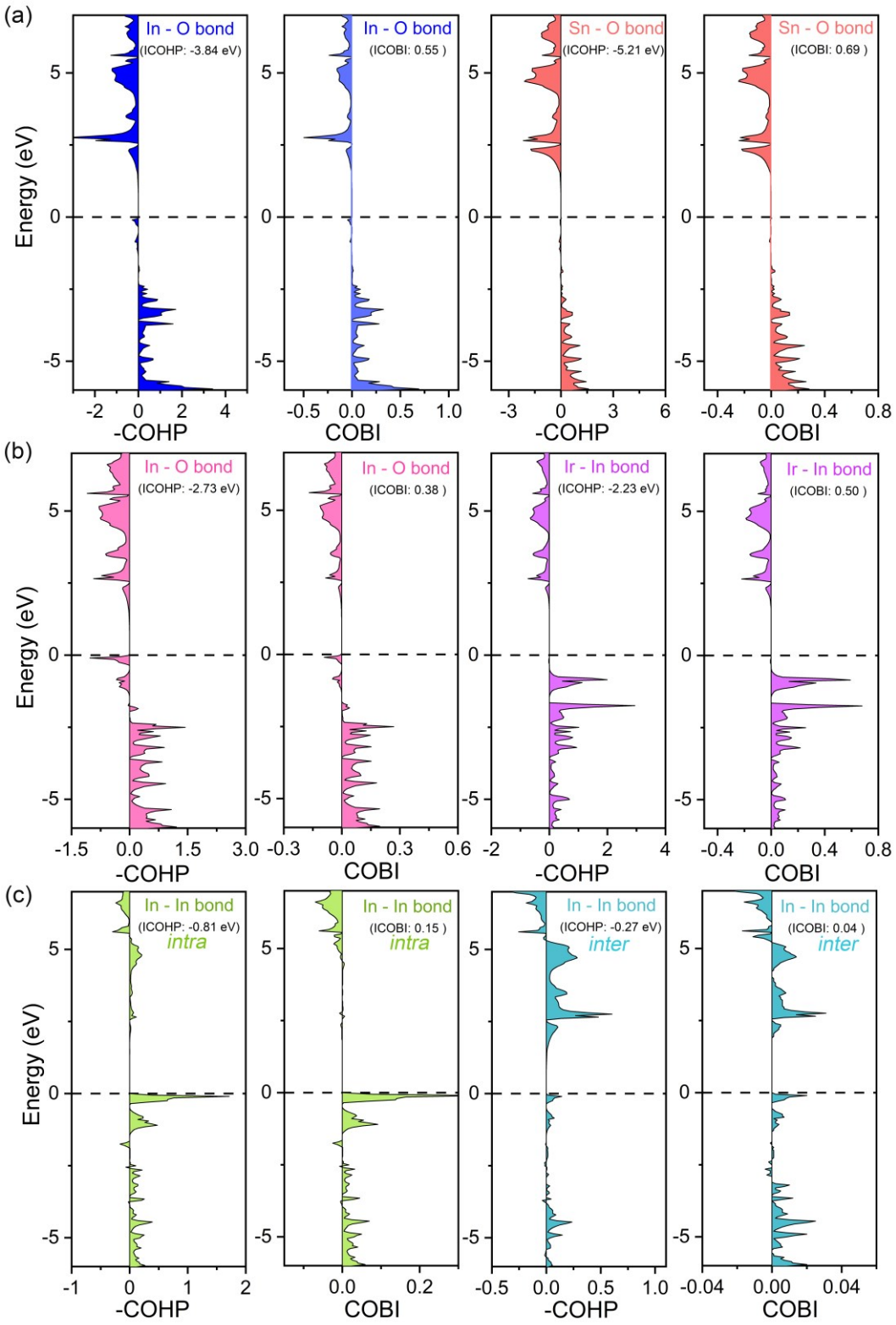

Figure S31. Calculated pCOHP (partial crystal orbital Hamilton population) and pCOBI (partial crystal orbital bond indices) of $IrIn_6InSnO_8$.

32. pCOHP and pCOBI of $IrIn_6InTiO_8$

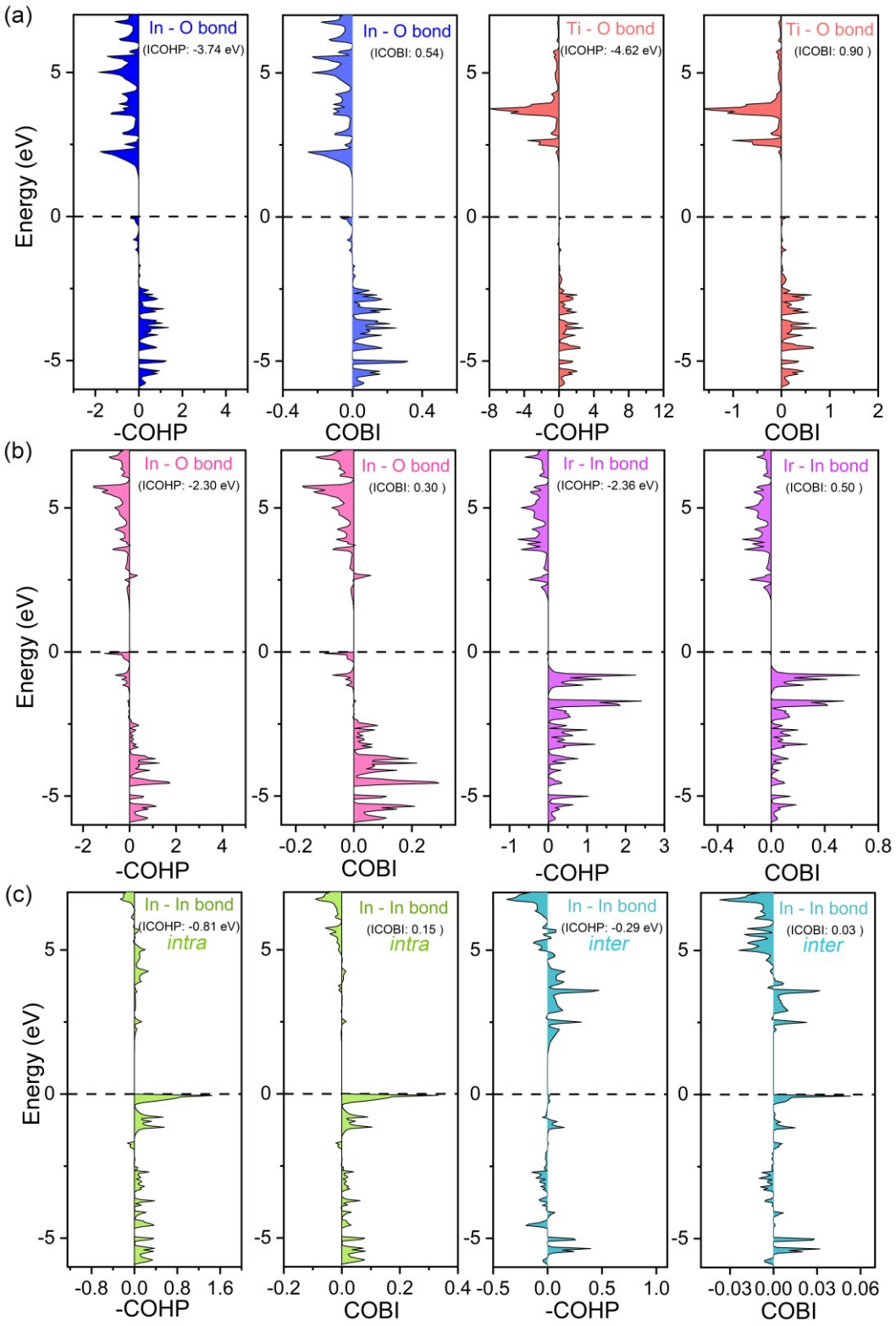

Figure S32. Calculated pCOHP (partial crystal orbital Hamilton population) and pCOBI (partial crystal orbital bond indices) of $IrIn_6InTiO_8$.

33. Orbital energies of In-5s, Sn-5s, Pb-6s, Bi-6s, and O-2p

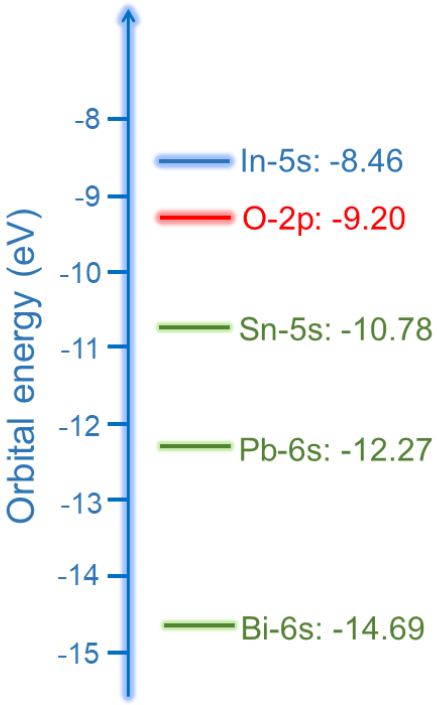

Figure S33. Orbital energies of In-5s, O-2p, Sn-5s, Pb-6s, and Bi-6s. The orbital energies were are obtained from NIST Standard Reference Database.

34. Real part and imaginary part of the dielectric function for $IrIn_6GaGeO_8$

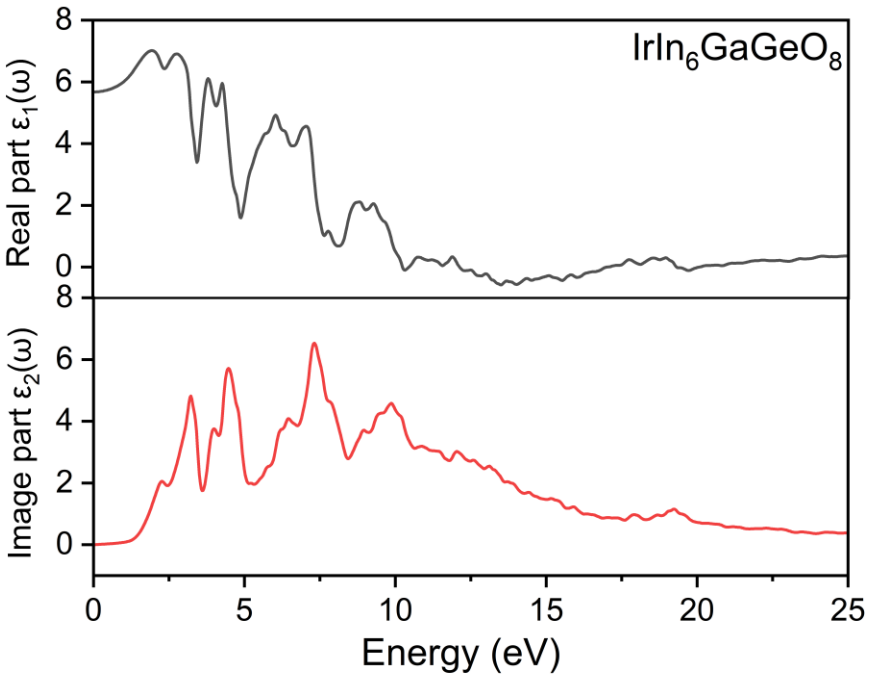

Figure S34. HSE06 calculated real part and imaginary part of the dielectric function for $IrIn_6GaGeO_8$.

35. Real part and imaginary part of the dielectric function for $IrIn_6GaSnO_8$

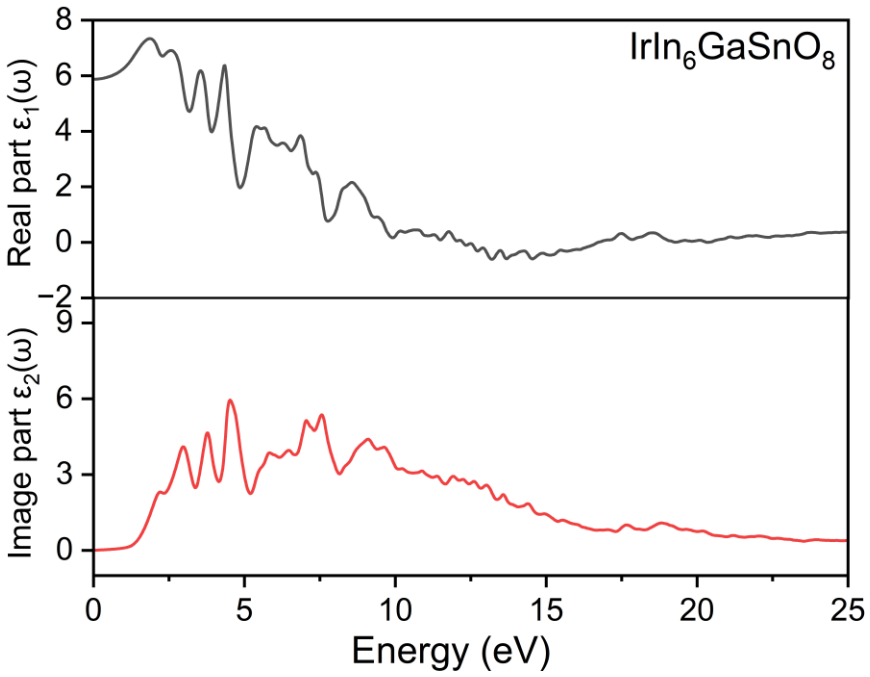

Figure S35. HSE06 calculated real part and imaginary part of the dielectric function for $IrIn_6GaSnO_8$.

36. Real part and imaginary part of the dielectric function for $IrIn_6GaTiO_8$

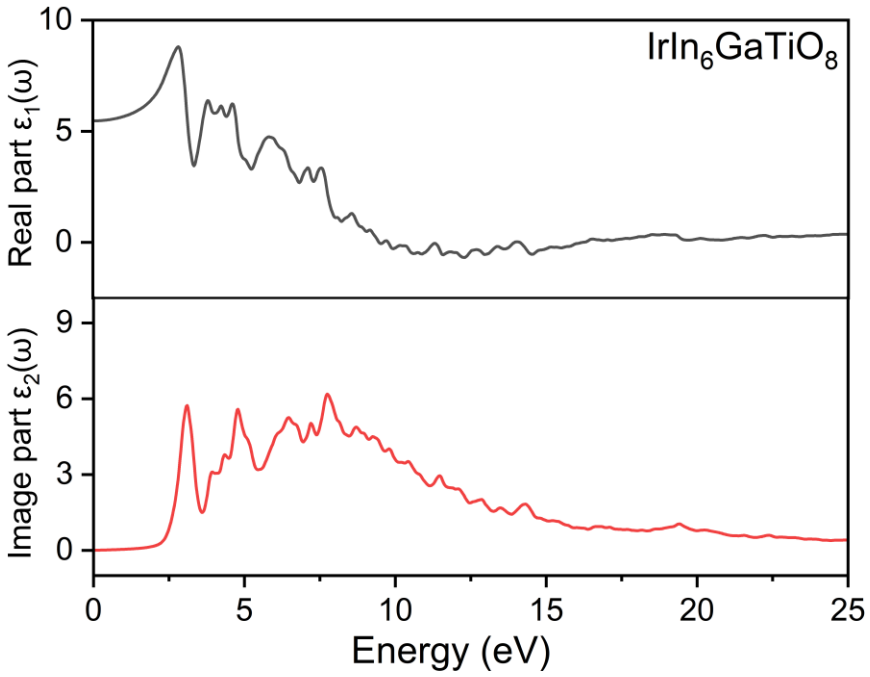

Figure S36. HSE06 calculated real part and imaginary part of the dielectric function for $IrIn_6GaTiO_8$.

37. Real part and imaginary part of the dielectric function for $IrIn_6InGeO_8$

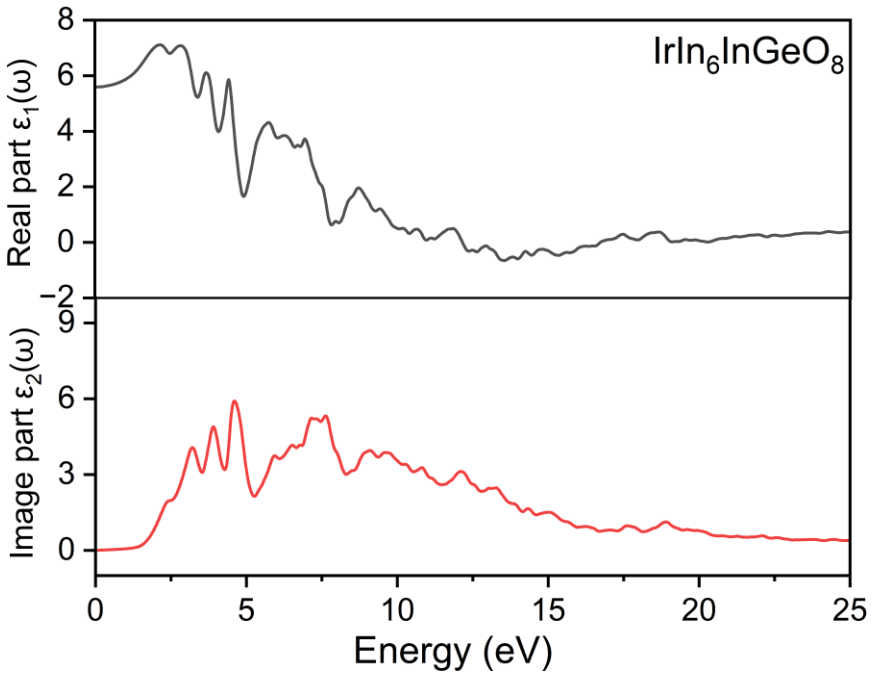

Figure S37. HSE06 calculated real part and imaginary part of the dielectric function for $IrIn_6InGeO_8$.

38. Real part and imaginary part of the dielectric function for $IrIn_6InSnO_8$

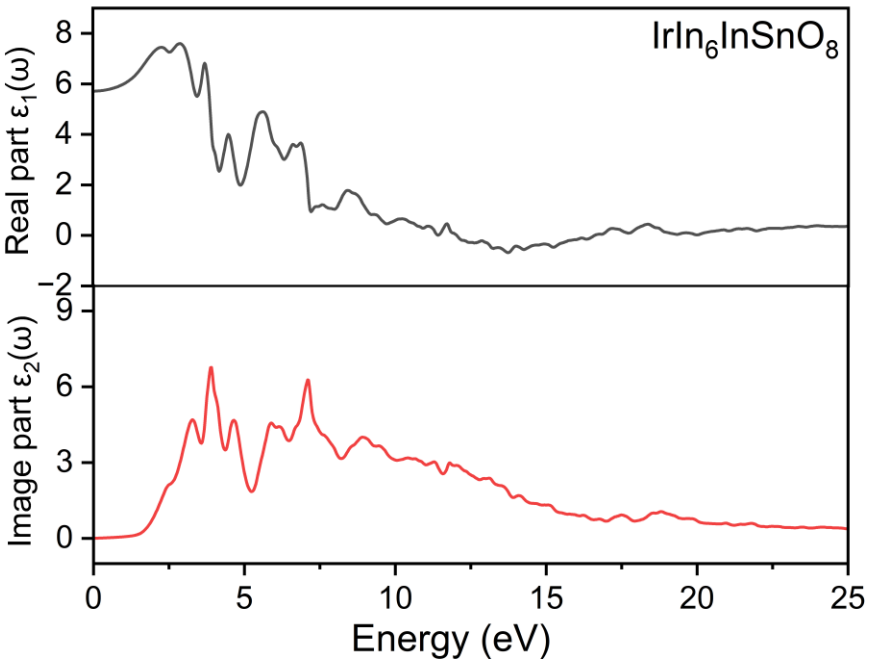

Figure S38. HSE06 calculated real part and imaginary part of the dielectric function for $IrIn_6InSnO_8$.

39. Real part and imaginary part of the dielectric function for $IrIn_6InTiO_8$

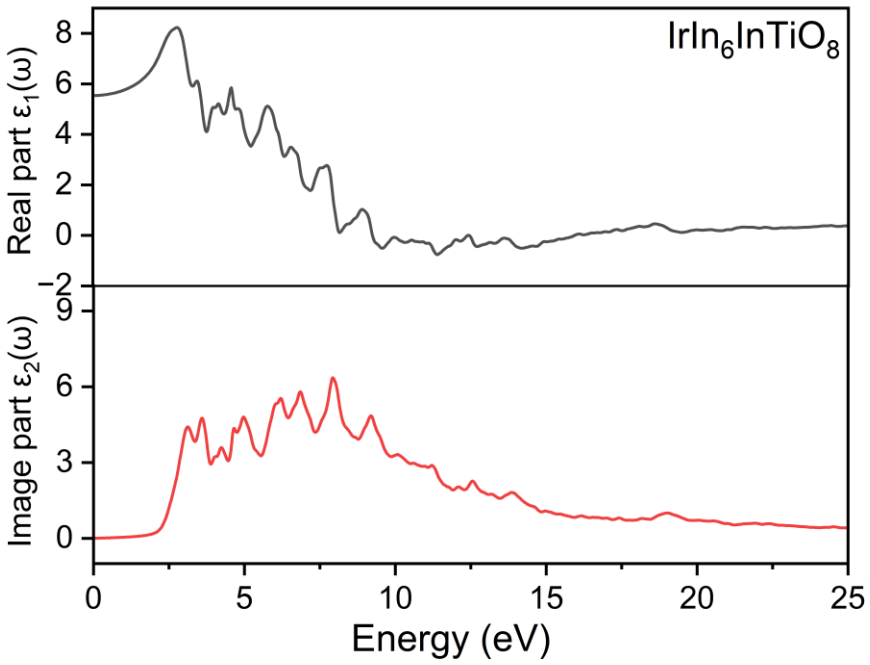

Figure S39. HSE06 calculated real part and imaginary part of the dielectric function for $IrIn_6InTiO_8$.

40. Table of cell parameter and bond lengths for $IrIn_6InGeO_8$

Table S1. Calculated and experimental cell parameter and bond lengths for $IrIn_6InGeO_8$ using PBE and PBE-sol functionals

	Lattice parameter		**Bond length**			
	a	error	Ir-In	In1-O	In2-O	Ge-O
PBE	10.31	1.87%	2.57	2.41	2.16	1.82
PBE-sol	10.19	0.69%	2.54	2.24	2.14	1.81
Experiment[1]	10.12	––	2.53	2.33	2.06	1.83

41. Table of elastic constant for $IrIn_6XYO_8$ (X = Ga, In; Y = Ge, Sn, Ti)

Table S2. Calculated elastic constant of $IrIn_6XYO_8$ (X = Ga, In; Y = Ge, Sn, Ti)

Compounds	C_{11} (GPa)	C_{12} (GPa)	C_{44} (GPa)
$IrIn_6GaGeO_8$	244.301	93.783	39.228
$IrIn_6GaSnO_8$	245.867	90.027	31.261
$IrIn_6GaTiO_8$	237.078	95.587	40.391
$IrIn_6InGeO_8$	240.160	89.091	35.501
$IrIn_6InSnO_8$	241.378	86.606	28.327
$IrIn_6InTiO_8$	233.217	89.324	34.166

42. Table of effective masses of carriers for $IrIn_6XYO_8$ (*X* = Ga, In; *Y* = Ge, Sn, Ti)

Table S3. Calculated effective masses of electron and hole along different directions around CBM and VBM for $IrIn_6XYO_8$ (*X* = Ga, In; *Y* = Ge, Sn, Ti)

Compounds	Direction	m_e^*/m_0	m_h^*/m_0
$IrIn_6GaGeO_8$	Γ→K	0.144	4.387
	Γ→L	0.144	5.732
$IrIn_6GaSnO_8$	Γ→K	0.151	43.961
	Γ→L	0.151	58.188
$IrIn_6GaTiO_8$	Γ→K	0.282	4.729
	Γ→L	0.284	5.994
$IrIn_6InGeO_8$	Γ→K	0.145	18.542
	Γ→L	0.145	3000.324
$IrIn_6InSnO_8$	Γ→K	0.138	37.070
	Γ→L	0.138	9.803
$IrIn_6InTiO_8$	Γ→K	0.275	3.916
	Γ→L	0.275	5.515

43. Table of electrical ε_∞, phonon vibrational ε_p and static ε_r dielectric constants of $IrIn_6XYO_8$ (X = Ga, In; Y = Ge, Sn, Ti)

Table S4. Calculated electrical ε_∞, phonon vibrational ε_p and static ε_r dielectric constants of $IrIn_6XYO_8$ (X = Ga, In; Y = Ge, Sn, Ti)

Compounds	ε_∞	ε_p	ε_r
$IrIn_6GaGeO_8$	27.297	8.294	35.591
$IrIn_6GaSnO_8$	36.718	8.411	45.129
$IrIn_6GaTiO_8$	8.524	7.119	15.643
$IrIn_6InGeO_8$	13.805	8.340	22.145
$IrIn_6InSnO_8$	13.705	7.712	21.417
$IrIn_6InTiO_8$	7.353	8.695	16.048

44. Table of exciton binding energy of $IrIn_6XYO_8$ (*X* = Ga, In; *Y* = Ge, Sn, Ti)

Table S5. Calculated exciton binding energy (E_b) of $IrIn_6XYO_8$ (*X* = Ga, In; *Y* = Ge, Sn, Ti)

Compounds	E_b / meV
$IrIn_6GaGeO_8$	-1.5
$IrIn_6GaSnO_8$	-1.0
$IrIn_6GaTiO_8$	-14.8
$IrIn_6InGeO_8$	-4.0
$IrIn_6InSnO_8$	-4.1
$IrIn_6InTiO_8$	-13.6

45. Table of Gibbs free energy of hydrogen adsorption (ΔG_{H^*}) for $IrIn_6XYO_8$ (X = Ga, In; Y = Ge, Sn, Ti)

Table S6. Calculated Gibbs free energy of hydrogen adsorption (ΔG_{H^*}) of $IrIn_6XYO_8$ (X = Ga, In; Y = Ge, Sn, Ti) at most stable adsorption site on different low-index lattice planes. E_{DFT} represents the lowest total energy for the surface with adsorbed hydrogen atoms among all H-adsorption configurations.

Photocatalysts	Lattice plane	E_{DFT}/eV	ΔG_{H^*}/eV	Adsorption site
$IrIn_6GaGeO_8$	(100)	-181.86	-0.43	2
	(110)	-182.82	-0.11	4
	(111)	-184.51	-0.05	12
$IrIn_6GaSnO_8$	(100)	-179.32	-0.40	2
	(110)	-181.34	-0.14	4
	(111)	-183.26	-0.26	10
$IrIn_6GaTiO_8$	(100)	-195.90	-0.40	2
	(110)	-195.70	-0.66	8
	(111)	-196.47	0.22	10
$IrIn_6InGeO_8$	(100)	-179.32	-0.42	1
	(110)	-180.68	-0.73	3
	(111)	-182.54	-0.10	10
$IrIn_6InSnO_8$	(100)	-176.52	-0.39	1
	(110)	-178.88	-0.63	3
	(111)	-181.01	-0.29	10
$IrIn_6InTiO_8$	(100)	-193.18	-0.38	1
	(110)	-193.68	-0.30	4
	(111)	-195.43	-0.65	9

References:

1. J. Kohler, H. A. Friedrich, C. Lee and M. H. Whangbo, *Z. Anorg. Allg. Chem.*, **2007**, *633*, 1464-1471.